Technical Internship :

Absorbing Boundary Layers in Time Domain Elastodynamics :

Two-Dimensional Perfectly Matched Layer

Computational Solid Mechanics Laboratory (LSMS)

Ecole Polytechnique Fédérale de Lausanne 2017-2018

Polytech Sorbonne 2017-2018

March 2018 - August 2018

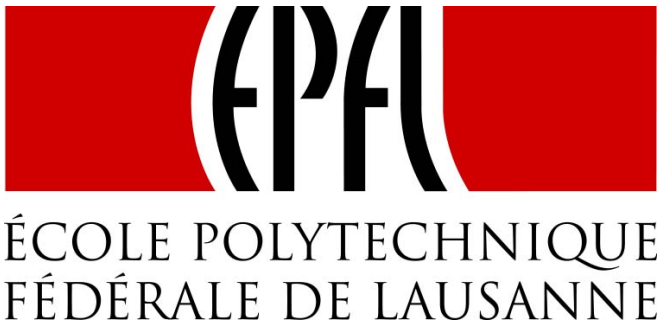

Student : Alexandre Poulain

Project supervisor : Michael Brun

Laboratory director : Jean-François Molinari

August 2018

Abstract

Absorbing boundary layers is a common method to solve numerically wave propagation phenomena in infinite or unbounded domains. Several techniques exist to construct these boundaries such as the introduction of Rayleigh damping in the absorbing layer or as presented in this report, perfectly matched layers (PML). They find their application in many fields such as electromagnetism and elastodynamics. Due to the complexity of the formulation of these PMLs, their construction and use remain a challenge. A large number of formulations and implementations have been proposed through the years to tackle some problems such as instability and performance. We attend in this report to present the formulation of a stable unsplit field two-dimensional perfectly matched layer based on the weak form of the equations of elastodynamics.

First of all, the presentation of the construction of the PML will be detailed, including an extensive description of the governing equations. During this description, we will also see how the PML is able to attenuate waves. This will be followed by the implementation of the scheme in Akantu : an open-source finite-element software developed in the Computational Solid Mechanics Laboratory of the EPFL. The algorithm with the main steps of the scheme will be presented. The numerical stability of the two dimensional unsplit field PML has never been demonstrated in the context of elastodynamics. Thus the method employed to prove the stability will be described and the results will be analyzed. The implicit and explicit schemes associated with the PML will be proved to be respectively unconditionally and conditionally stable. Some of the key features of the PML will also be highlighted by this analysis, such as the postponing of the critical time step, for which the explicit scheme becomes unstable. The results on two test cases will be reviewed in the last part of this report and a special attention will be dedicated to the reflection of the waves since this parameter represents the efficiency of the PML. For both test cases, a non-harmonic wave is injected within the domain of interest and it is characterised by a Ricker wave. The first test case is the simplest one and will be used to confirm the ability of the PML to attenuate incident wave. It is composed of a bar separated in two parts : an elastic medium and a PML. We will shortly see that the scheme is efficient to attenuate incident waves with less than 1 percent of the incident wave reflected. The second test case is a well known study case for seismic wave : the Lamb's test. It involves 3 types of wave : pressure, shear and Rayleigh waves. This latter wave is a powerful surface wave, but it will be attenuated by the PML in a very efficient manner. Once again the efficiency of the PML will be estimated to less than 1% of incident wave reflected by the truncation interface. To be able to use the PML and to fit a specific simulation some advices will be given in this part.

Using the open source library Akantu, the reader is strongly advised to download the code and run the example presented in this report. In fact, they will constitute to the reader a good way to get hands-on training with Akantu and the PML method at the same time.

Résumé

La méthode des bords absorbants est un concept utilisé en simulation numérique pour modéliser la propagation d'ondes en milieu infini. Plusieurs formulations et techniques existent pour construire ces bords. Par exemple, l'introduction d'une atténuation de type Rayleigh ou, comme présenté dans ce rapport, la méthode des couches parfaitement adaptées (PML : Perfectly matched layers). Ces techniques trouvent leur application dans de nombreux domaines comme l'éléctromagnétisme ou l'élastodynamique. A cause de la complexité de la formulation de ces PML, leurs construction et utilisation restent difficiles en pratique. Plusieurs formulations et implémentations ont été proposées pour résoudre certains problèmes comme l'instabilité ou même pour améliorer les performances. Le but de ce rapport est de présenter la formulation stable de couches parfaitement adaptées à des problèmes en élastodynamique et à deux dimensions.

Dans un premier temps, la description complète et détaillée des équations régissant les PML sera faite. Nous partirons des équations du mouvement simple et par l'introduction de fonctions d'étirement, nous serons en mesure de formuler la forme forte des PML. S'inscrivant dans le contexte des éléments finis, la forme faible de ces équations sera décrite et partant de là nous présenterons sa formulation discrète en temps et en espace. L'implémentation de ce schéma numérique sera effectuée dans le logiciel Akantu qui est une librairie open source pour le calcul numérique dans la méthode des éléments finis. Cette librairie est développée au sein du Laboratoire de Simulation en Mécanique des Solides de l'Ecole Polytechnique Fédérale de Lausanne. Bien que ce schéma existe dans la littérature, il n'a jamais été implémenté et mis à disposition de manière open source. De plus, de nombreuses analyses de stabilité de schémas associés à des PML ont été effectuées mais cette formulation, bien qu'elle présente de nombreux avantages, n'a jamais été prouvée stable. Dans un second temps, nous étudierons donc la stabilité du schéma numérique précédemment décrit. Les schémas implicite et explicite seront analysés et seront prouvés respectivement inconditionnellement et conditionnellement stables. Certaines propriétés de ce schéma seront mis en exergue lors de cette analyse de stabilité comme par exemple la faculté que le schéma explicite possède à repousser la limite de stabilité imposée par le pas de temps critique. La dernière partie de ce rapport sera consacrée à la présentation et l'analyse de résultats numériques. Deux cas tests seront décrits : le premier est une simplification du problème à un cas uni-dimensionnel et le second est le cas test de Lamb. Une attention particulière sera portée à la réflexion de l'onde due à l'interface entre le milieu élastique et la PML. L'onde imposée en entrée est une onde de Ricker qui est une onde non-harmonique. Le premier cas test est constitué d'une barre et permet de montrer la capacité d'atténuation des ondes des PML. Nous serons en mesure de montrer que la PML permet d'atténuer plus de 99% de l'onde incidente. La réflexion de l'onde due à l'interface entre les deux sous-domaines peut être minimisée par certains choix effectués au niveau des paramètres de la PML. Le test de Lamb permet de soumettre la PML à test bien connu des sismologues : la propagation d'une onde sismique dans un domaine supposé infini. Sans PML, l'analyse de l'onde est perturbée par sa réflexion aux bords du domaine. Une nouvelle fois la PML ne permettra la réflexion que de moins d'1% de l'onde incidente. Le futur utilisateur de la PML recevra dans cette dernière partie quelques conseils sur le choix des paramètres de la PML afin de minimiser cette réflexion indésirable et pour maximiser les performances du schéma numérique.

Acknowledgments

First and foremost, I want to express my gratitude to Jean-François Molinari, director of the Computational Solid Mechanics Laboratory (LSMS) to have believed in my capacities and to have followed all stages of my works. For his expertise in the field of perfectly matched layers and coupling methods, I want to thank warmly Michael Brun, invited professor at LSMS. His numerous advices and feedbacks have greatly enriched this work. The analysis of the results of stability mainly due to the guidance of M. Brun. For their help concerning Akantu and the implementation of this project, I want to thank Guillaume Anciaux and Nicolas Richart, respectively research associate at LSMS and HPC application expert at Scitas. Their recommendations guided me during the process of coding the PML method within Akantu in an efficient manner, taking advantage of the different features the library.

Table des matières

Introduction

The study of wave propagation in unbounded media is a growing topic of research and takes its applications in many engineering fields. The solution of the elastodynamic problem using infinite domains is interesting for the simulation of earthquake ground motion or for soil-structure problems where the reflection of the wave at the boundaries needs to be eliminated. To address this problem, a common practice is to add a layer surrounding the domain of interest in order to absorb the outgoing wave.
Different methods have been developed to simulate wave propagation in unbounded media : the infinite element methods, originally developed by Ungless [29] and Bettess [26], which is close to the concept of finite elements but adds a new formulation including an infinite extent of the element region and shape functions. This method allows the approximation of the decaying laws governing the waves radiation process at infinity. The technique used here is to use finite element with their end nodes placed at infinity. The issues encountered with such technique is the same as the following method. The appropriate absorbing boundary conditions is a method involving specific conditions at the model boundaries to approximate the radiation condition for elastic waves [4]. The definition of these boundaries using this method leads to non stable schemes and spurious reflections cannot be avoided. These conditions are also not useful for practical calculations since they involve a complex system of equations. The two first methods presented here present the same drawbacks in terms of computation and analysis. However, in order to solve the same problems other methods have been developed leading to more efficient schemes.
As presented in this report, another method is to define a new layer to the simulation : An absorbing layer. The Rayleigh Damping layer is based on a Rayleigh/Caughey damping formulation to express the damping matrix $[C]$ in the classic formulation of elastodynamic problems. This damping matrix in the Rayleigh formulation can be expressed as a combination of stiffness and mass matrix. This damping matrix, in the context of the finite element method, is often already available in existing Finite Element software which makes this method really practical to use. In [31], the efficiency of the method is given and shows a satisfactory behaviour of the method in terms of efficiency of the one and the two dimensional case.
Perfectly matched layers are another absorbing boundary layers method, that absorbs almost perfectly incident waves without any reflection from the truncation interface for all angles of incidence and frequencies. The wave entering into the PML decays with distance according to a user-defined decay function. The property of the non-reflection at the truncation interface is true in theory for the continuum case. Once a spatial discretization is used, numerical reflections are present, but they can be attenuated using the parameters of the PML. These user-defined parameters can also increase the accuracy of the scheme used and even reduce the computational cost.
Perfectly matched layers is a concept first introduced by Bérenger for the simulation of electromagnetic waves [20]. He used a split-field formulation and it arises from the use of complex-valued coordinate stretching in the electromagnetic wave equations [11]. The field-splitting formulation permits to avoid convolutional operations in the time domain when the resulting forms are inverted back into the frequency domain. It is based on the partition of the variables into two components : parallel and perpendicular to the truncation boundary. The drawback of this technique is that it alters the structure of the underlying differential equations and thus increases the number of unknowns. Another problem with Bérenger's split-field PML is that the problem is only weakly well-posed and thus prone to instability [2]. This led to the development of strongly well-posed unsplit formulation [1] but it turns out that these formulations also suffer from instability and need further manipulation of the equations to ensure it [3]. However, PML have been adapted for other linear wave equations such as the Helmholtz equation (scalar wave equation) [28, 34, 18], linearised Euler equations [17] or for the wave propagation in poroelastic materials [38]. An extensive discussion of these different methods is beyond the scope of this report since we focus on elastodynamic problems.
Indeed, the concept of PML was first adapted to elastodynamic wave propagation problems by Hastings

et al [19]. This formulation was obtained by taking the split-field formulation of Bérenger and directly applying it to the P- and S-wave potentials. This formulation was obtained in term of displacement potentials and yields to a velocity-stress finite-difference method. The proof of the absorptive property of the PML was developed by Chew and Liu [10] : they developed at the same time a new split-field formulation for isotropic media using complex-valued coordinate stretching to obtain the equations governing the PML. Following the same idea Liu [27] introduced a split-field PML for time-dependent elastic waves in cylindrical and spherical coordinates. Other split-field, time-domain PML for the velocity–stress formulation have been obtained and we refer to [39, 13, 9] for the details of these methods and the presentation of a finite-differences-time-domain (FDTD) implementation of them. Another split-field formulation was introduced by Komatitsch and Tromp [21] where the stress term is eliminated and the displacement is split into four components. This results in a third-order in time semi-discrete forms for the four displacement fields or can be expressed by a second-order system coupled with one first-order equation for one of the displacement field. The main drawback of their method is its complexity, but it is the first displacement only formulation for elastodynamics.

As we have seen before split-field PML suffer from instability since they are weakly well-posed. Wang [36] introduced an unsplit formulation for finite-difference modeling of elastic wave propagation using convolution features (CPML). In contrast of the original formulation of CPML from the electromagnetic where they used complex-frequency-shifted stretching functions [33, 30], Wang used standard stretching functions for its PML implementation. In this report, we will develop an unsplit formulation using the finite element framework in the same spirit as Basu and Chopra. In [5], they introduced an unsplit-field PML for time-harmonic elastodynamics in 2D media. In [6], they developed the time-domain implementation of their PML and in [35], Basu extended its 2D formulation to 3D media using an explicit scheme.

Based on a decomposition of the elastodynamics equations as a first-order system, Cohen and Fauqueux [12] derived a split-field formulation where the strain tensor is split and they had to introduce independent stress variables to account for the split strain tensor components. This method was implemented using a mixed finite element approach and spectral elements. A different formulation was obtained by Festa and Vilotte [16] where they followed classic lines for reducing the second-order displacement-only elastodynamic problem to a first-order in time system. Instead of slitting the strain tensor, they used split-fields for both the velocity and stress components. In the framework of unsplit PML, Drossaert and Giannopoulos [15] described an alternative implementation based on recursive integration (RIPML). But this implementation presents less performance than the CPML for elastodynamics using the complex-frequency-shifted stretching functions[14]. Meza-Fajardo and Papageorgiou [25] discussed a novel PML approach. In the standard approach of PML the coordinate-stretching and associated decay functions are used along the direction normal to the PML interface. Meza-Fajardo and Papageorgiou introduced them along all coordinate directions resulting in a split-field, non-convolutional M-PML which shows superior performance compared to standard PML.

All this literature survey of the different formulation of the PML can be summarised in the following table borrowed from [22] :

Table 1 – PML implementations in time-domain elastodynamics

Implementation	split-field	unsplit-field
FD	Chew and Liu [10]	Wang and Tang [36]
	Hastings et al. [19]	Drossaert and Giannopoulos [15, 14]
	Liu[27]	Komatitsch and Martin [21]
	Collino and Tsogka [13]	
FE/SE	Bécache et al. [9]	Basu and Chopra [5]
	Komatitsch and Tromp [21]	Basu [6]
	Cohen and Fauqueux [12]	
	Festa and Vilotte [16]	
	Meza-Fajardo and Papageorgiou [25]	

The stability of the PML has been studied for mostly isotropic cases, but Collino and Tsogka [13] showed that the split-field standard PML is adequate in the case of anisotropic conditions. Also Bécache [8] studied the stability of the PML and the effect of anisotropy : She showed that the standard PML is stable for isotropic cases and conditionally unstable for anisotropic applications. Bécache also proposed necessary conditions for stability in the form of inequalities choice of the stretching function.

In the light of these previous works we will attend in this report to describe the formulation of a two dimensional unsplit-field displacement-based PML. The implementation will be realised in the framework of finite elements and using the open source finite element library Akantu. This software is developed in the Computational Solid Mechanics Laboratory of the EPFL. Proposing the PML method as a feature of Akantu will permit to simulate numerically two dimensional wave propagation on unbounded domains. PML have never been proposed in an open source library since then. Of course before implementing such method, a careful analysis must be done. One of the key elements is the numerical stability. The user must be sure that he can run long time simulations without experiencing any unstability from features of Akantu. That is why we propose in this report a numerical stability analysis of the PML implemented in Akantu. In the last part of this report, we will review the numerical results obtained on two test cases. The first one is a simple bar and the second is the Lamb test. These test cases are also implemented as examples in Akantu. The user will be able to retrivee the results shown in this report before using the PML for his own projects.

1 Description

1.1 Elastic medium

As an introduction of the governing equations, let us describe the elastic medium since the PML is surrounding it. In fact the construction of the PML relies on the same governing equations as the physical medium and share some parameters with it.
Let us consider an isotropic homogeneous elastic medium under plane-strain motion and without body forces. The motion in the medium is governed by :

$$\begin{cases} \sum_j \frac{\partial \sigma_{ij}}{\partial x_j} & = \rho \ddot{u}_i \\ \sigma_{ij} & = \sum_{k,l} C_{ijkl} \epsilon_{kl} \\ \epsilon_{ij} & = \frac{1}{2}\left(\frac{\partial u_i}{\partial x_j} + \frac{\partial u_j}{\partial x_i}\right) \end{cases} \tag{1}$$

With $u(x,t)$ the displacement, ϵ the strain, σ the stress, ρ the mass density of the medium. C is the material stiffness tensor and its components are expressed in term of the Kronecker delta δ_{ij} :

$$C_{ijkl} = (\kappa - \frac{2}{3}\mu)\delta_{ij}\delta_{kl} + \mu(\delta_{ik}\delta_{jl} + \delta_{il}\delta_{jk}) \tag{2}$$

Where κ is the bulk modulus and μ the shear modulus.
If we consider an unbounded domain, the system 1 admits solutions of the form of P- waves and S-waves. The solutions of P-waves have the following formulation :

$$u(x,t) = q \exp(-ik_p x.p) \exp(i\omega t) \tag{3}$$

with $k_p = \frac{\omega}{c_p}$ where ω is the frequency of the wave and $c_p = \sqrt{(\kappa + 4\mu/3)/\rho}$ which is the celerity of the P-wave. In the equation 3 p denotes the unit vector pointing in the direction of propagation of the wave and $q = \pm p$. The solution of S-wave form take the following formulation :

$$u(x,t) = q \exp(-ik_s x.p) \exp(i\omega t) \tag{4}$$

Where $k_s = \omega/c_s$ and the S-wave speed is $c_s = \sqrt{\mu/\rho}$ and $q.p = 0$.

1.2 Strong form in frequency domain

Before describing the governing equations of the two-dimensional PML let us introduce the following notations : Ω_{PML} will denote the PML domain which is bounded by $\Gamma_{PML} = \Gamma^D_{PML} \cup \Gamma^N_{PML}$. Γ^D_{PML} corresponds to the boundary where the Dirichlet condition are applied (imposed displacement). Γ^N_{PML} is the boundary where the tractions are applied and represents the boundary of the Neumann conditions. The intersection of these two boundaries defined by the imposed conditions is null : $\Gamma^D_{PML} \cap \Gamma^N_{PML} = \emptyset$. The temporal domain will be denoted by $J = [0, T]$ with T the end time.
The classical formulation of PML begins with the introduction of the complex-valued coordinates stretching functions λ_i. They are used to replace the real coordinates by the complex ones : $x_i \to \tilde{x}_i : \mathbb{R} \to \mathbb{C}$.

$$\lambda_i(x_i) = \frac{\partial \tilde{x}_i}{\partial x_i} = 1 + f^e_i(x_i) - \frac{i}{bk_s} f^p_i(x_i) \tag{5}$$

where b is the characteristic length of the problem. $k_s = \omega/c_s$ denotes the wavenumber (ω is the pulsation and c_s is the celerity of shear waves). i is used to denote the direction x or y. f^p_i and f^e_i are the attenuation functions for respectively propagating and evanescent waves. They are written as a polynomial of order n.

$$f^\alpha_i = a_\alpha \left(\frac{x_i - x_0}{L_{p,i}}\right), x_i \in [x0, x0 + d] \tag{6}$$

The tunable property of the PML relies mainly on the formulation of the attenuation functions. The value of the coefficients of attenuation a_p, a_e, the order of the polynomial n, and the size of the PML L_p can be defined by the user. As we will see in the section concerning the numerical results, these parameters need to be chosen carefully and depending on the problem to obtain the "best" result possible. The concept of "best result" depends on the expectations of the user. Accuracy versus performance is a deep-seated problem for all numerical simulations. The perfectly matched layer does not get out of this rule. In order to choose the value of these coefficients, we can use the reflection coefficient for an incident pressure wave given by [6] :

$$R_{pp} = \frac{cos(\theta + \theta_s)}{cos(\theta - \theta_s)} \exp\left[-2\frac{c_s}{c_p} F_1(L_p) cos(\theta)\right] \tag{7}$$

Where c_p stands for the velocity of P-waves. The incident P-wave is characterised by θ, its angle of incidence and θ_s, its reflective angle after being reflected at the end of the PML. F_1 corresponds to the integral over the PML of the attenuation function for propagating waves : $F_1(L_p) = \int_{s=0}^{L_p} f^p(s)ds = \frac{\beta_0 L_p}{n+1}$. Thus, the attenuation coefficients can be expressed in function of the reflection coefficient :

$$a_\alpha = \ln\left(\frac{cos(\theta + \theta_s)}{R_{pp} cos(\theta - \theta_s)}\right) \frac{c_p}{c_s} \frac{n+1}{L_p cos(\theta)} \tag{8}$$

If we consider that the incident wave has an angle of $\theta = \theta_s = 0$ therefore the value of the coeffecient has the form :

$$a_\alpha = \ln\left(\frac{1}{R_{pp}}\right) \frac{c_p}{c_s} \frac{n+1}{L_p cos(\theta)} \tag{9}$$

Using the complex-valued coordinates stretching functions 5, the strong form of the equations of motion for the PML in the frequency domain is defined by :

$$\begin{cases} \sum_j \frac{1}{\lambda_j(x_j)} \frac{\partial \sigma_{ij}}{\partial x_j} & = -\omega^2 \rho u_i \\ \sigma_{ij} & = \sum_{k,l} C_{ijkl} \epsilon_{kl} \\ \epsilon_{ij} & = \frac{1}{2}\left(\frac{1}{\lambda_j(x_j)} \frac{\partial u_i}{\partial x_j} + \frac{1}{\lambda_i(x_i)} \frac{\partial u_j}{\partial x_i}\right) \end{cases} \tag{10}$$

Where C_{ijkl} are the components of the elastic constitutive tensor. In fact the system 10 defines a perfectly matched medium (PMM) and the elastic medium is just a specific case of PMM with $\lambda_j(x_j) = 1$, $\forall x \in \Omega_{PML}$. If we imagine a PML, surrounding an elastic medium, as in the figure 1, we have to define for the PML $\lambda_j(x_j) = 1$ for $\forall x \in \Gamma_{PML}$ at the interface between the two-subdomains.
The system of equations 10 assumes harmonic time-dependence of the displacement, stress and strain. Therefore, its solution can be written as $u(x,t) = \overline{u}(x,t) exp(i\omega t)$. If the stretching functions have the formulation 5 then the system 10 has solutions of the form :

$$\overline{u}(x) = \exp[-\frac{c_s}{c_p} \sum_i F_i(x_i) p_i] q \exp(i k_p x.p) \tag{11}$$

with $q = \pm p$, and

$$\overline{u}(x) = \exp[-\sum_i F_i(x_i) p_i] q \exp(-i k_s x.p) \tag{12}$$

with $q.p = 0$ and $F_i(x_i) = \int_0^{x_i} f_i(\xi) d\xi$.
Therefore the solution admitted in the PML corresponds to the solution of the system 1 but with an imposed spatial attenuation. The attenuation contained in the term $\exp[-F_i p_i]$ for the direction i is independent of the frequency if the direction of propagation is.

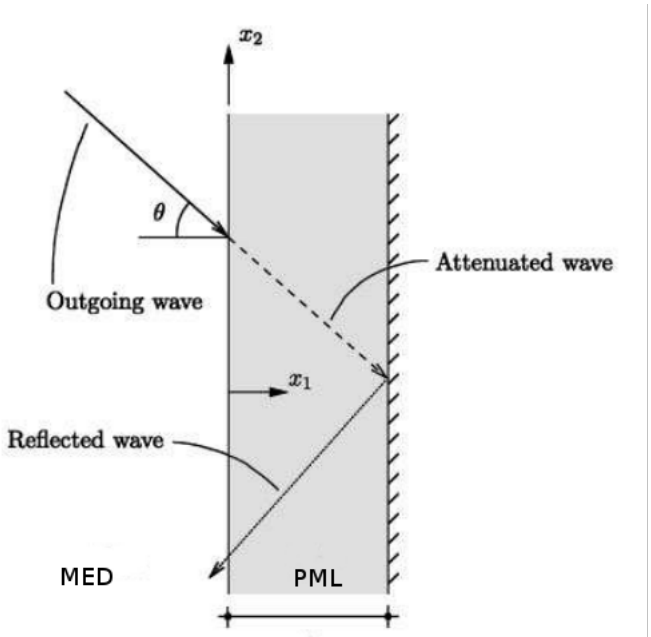

FIGURE 1 – Scheme of the propagation of a wave within the elastic medium (on the left) and the PML (on the right)

1.3 Strong form in time domain

The strong form of the PML in the temporal domain can be obtained by inverse Fourier transform of each equation of 10. Indeed the introduction of the complex-valued coordinates stretching functions makes the application of this inverse easier. In the following equation the number of lines below a tensor will specify its order.

$$\begin{cases} div(\underline{\underline{\sigma}}\tilde{F}^e + \underline{\underline{\Sigma}}\tilde{F}^p) = \rho f_m \ddot{\underline{u}} + \rho \frac{c_s}{b} f_c \dot{\underline{u}} + \frac{\mu}{b^2} f_k \underline{u}, & \text{In } \Omega_{PML} \times J \\ \underline{\underline{\sigma}} = C : \underline{\underline{\epsilon}}, & \text{In } \Omega_{PML} \times J \\ F^{eT}\dot{\underline{\underline{\epsilon}}}F^e + F^{pT}\underline{\underline{\epsilon}}F^e + F^{eT}\underline{\underline{\epsilon}}F^p + F^{pT}\underline{\underline{\underline{E}}}F^p = ... & \\ \frac{1}{2}(\nabla\dot{\underline{u}}^T F^e + F^{eT}\nabla\dot{\underline{u}}) + \frac{1}{2}(\nabla\underline{u}^T F^p + F^{pT}\nabla\underline{u}), & \text{In } \Omega_{PML} \times J \end{cases} \tag{13}$$

submitted to the homogeneous boundary conditions :

$$\begin{cases} \underline{u} = 0, & \text{on } \Gamma^D_{PML} \\ (\underline{\underline{\sigma}}\tilde{F}^e + \underline{\underline{\Sigma}}\tilde{F}^p).n, & \text{on } \Gamma^N_{PML} \end{cases} \tag{14}$$

Let us now summarize the form of the different matrices $F^e, F^p, \tilde{F}^e$ and $\tilde{F}^p$ of the above equations.

$$F^e = \begin{bmatrix} 1 + f_1^e(x1) & 0 \\ 0 & 1 + f_2^e(x2) \end{bmatrix}, F^p = \begin{bmatrix} \frac{c_s}{b} f_1^p(x1) & 0 \\ 0 & \frac{c_s}{b} f_2^p(x2) \end{bmatrix} \tag{15}$$

$$\tilde{F}^e = \begin{bmatrix} 1 + f_2^e(x2) & 0 \\ 0 & 1 + f_1^e(x1) \end{bmatrix}, \tilde{F}^p = \begin{bmatrix} \frac{c_s}{b} f_2^p(x2) & 0 \\ 0 & \frac{c_s}{b} f_1^p(x1) \end{bmatrix} \tag{16}$$

Let us now focus on the first equation of 13, the functions f_m, f_c and f_k depend on the attenuation functions :

$$\begin{cases} f_m = (1 + f_1^e(x1))(1 + f_2^e(x2)) \\ f_c = (1 + f_1^e(x1))f_2^p(x2) + (1 + f_2^e(x2))f_1^p(x1) \\ f_k = f_1^p(x_1)f_2^p(x_2) \end{cases} \tag{17}$$

The next elements to define, which appear in the first and the third equations of 13 are the integral of the stress and the strain.

$$\underline{\underline{\Sigma}} = \int_0^t \underline{\underline{\sigma}} dt, \underline{\underline{E}} = \int_0^t \underline{\underline{\epsilon}} dt \tag{18}$$

1.4 Displacement-based weak form

Let us introduce the test function $\underline{v}$ belonging to an admissible space of solution V. Premultiplying the first equation of the strong form 13 by $\underline{v}$ and integrating over the PML domain gives :

$$\int_{\Omega_{PML}} \underline{v}.div(\underline{\underline{\sigma}}\tilde{F}^e + \underline{\underline{\Sigma}}\tilde{F}^p)d\Omega_{PML} = \int_{\Omega_{PML}} \rho f_m \underline{v}.\underline{\ddot{u}} d\Omega_{PML} + ... \\ \int_{\Omega_{PML}} \rho \frac{c_s}{b} f_c \underline{v}.\underline{\dot{u}} d\Omega_{PML} + \int_{\Omega_{PML}} \frac{\mu}{b^2} f_k \underline{v}.\underline{u} d\Omega_{PML}, \text{In } \Omega_{PML} \times J \tag{19}$$

Using the Gauss divergence theorem and integration per parts gives :

$$\int_{\Gamma_{PML}} \underline{v}.\left(\underline{\underline{\sigma}}\tilde{F}^e + \underline{\underline{\Sigma}}\tilde{F}^p\right).\underline{n} d\Gamma_{PML} = \int_{\Omega_{PML}} \rho f_m \underline{\ddot{u}}.\underline{v} d\Omega_{PML} + ... \\ \int_{\Omega_{PML}} \rho \frac{c_s}{b} f_c \underline{\dot{u}}.\underline{v} d\Omega_{PML} + \int_{\Omega_{PML}} \frac{\mu}{b^2} f_k \underline{u}.\underline{v} d\Omega_{PML} + \int_{\Omega_{PML}} \underline{\underline{\tilde{\epsilon}}}^e : \underline{\underline{\sigma}} d\Omega_{PML} + \int_{\Omega_{PML}} \underline{\underline{\tilde{\epsilon}}}^p : \underline{\underline{\Sigma}} d\Omega_{PML}, \text{In } \Omega_{PML} \times J$$

$\underline{n}$ is the vector normal to the boundary of the PML Γ_{PML}. The tensors $\underline{\underline{\tilde{\epsilon}}}^p$ and $\underline{\underline{\tilde{\epsilon}}}^e$ depend on the attenuation functions :

$$\begin{cases} \underline{\underline{\tilde{\epsilon}}}^e = \frac{1}{2}\left(\nabla \underline{v}\tilde{F}^e + \tilde{F}^{eT}\nabla \underline{v}^T\right) \\ \underline{\underline{\tilde{\epsilon}}}^p = \frac{1}{2}\left(\nabla \underline{v}\tilde{F}^p + \tilde{F}^{pT}\nabla \underline{v}^T\right) \end{cases} \tag{20}$$

Using the weak form of the equation of motion within the PML in the temporal domain 19 we can define the mass, damping and stiffness matrices :

$$m^e = \int_{\Omega_e} \rho f_m N_I N_J d\Omega_e I_d \tag{21}$$

$$c^e = \int_{\Omega_e} \rho f_c \frac{c_s}{b} N_I N_J d\Omega_e I_d \tag{22}$$

$$k^e = \int_{\Omega_e} \frac{\mu}{b^2} f_k N_I N_J d\Omega_e I_d \tag{23}$$

In the above equation N_I is the nodal shape function for node I. Let us introduce a notation for the internal forces term :

$$p^e = \int_{\Omega_{PML}} \underline{\underline{\tilde{\epsilon}}}^e : \underline{\underline{\sigma}} d\Omega_{PML} + \int_{\Omega_{PML}} \underline{\underline{\tilde{\epsilon}}}^p : \underline{\underline{\Sigma}} d\Omega_{PML} \tag{24}$$

In order to modify this term we need to make a temporal discretization.

1.5 Complete discrete form

Before describing the complete discrete equations of two-dimensional PML featuring the discretization in space and time, we need to introduce the following notation. The hat notation above an element will specify that the tensor is written in Voigt notation. For example $\hat{\sigma} = \begin{pmatrix} \sigma_{11} \\ \sigma_{22} \\ \sigma_{12} \end{pmatrix}$ Thus, using a simple temporal discretization with $dt = t_{n+1} - t_n$ we can rewrite the internal forces at time t_{n+1} as :

$$p^e_{n+1} = \int_{\Omega_e} \tilde{B}^{eT} \hat{\sigma}_{n+1} d\Omega_e + \int_{\Omega_e} \tilde{B}^{pT} \hat{\Sigma}_{n+1} d\Omega_e \tag{25}$$

The two matrices $\tilde{B}^p$ and $\tilde{B}^e$ in 25 depend on the nodal shape functions and the attenuation functions. They are expressed in term of their nodal submatrices as :

$$\tilde{B}^e_I = \begin{bmatrix} \tilde{N}^e_{I1} & 0 \\ 0 & \tilde{N}^e_{I2} \\ \tilde{N}^e_{I2} & \tilde{N}^e_{I1} \end{bmatrix}, \tilde{B}^p_I = \begin{bmatrix} \tilde{N}^p_{I1} & 0 \\ 0 & \tilde{N}^p_{I2} \\ \tilde{N}^p_{I2} & \tilde{N}^p_{I1} \end{bmatrix} \tag{26}$$

with

$$\tilde{N}^e_{Ii} = \tilde{F}^e_{ji} N_{I,j}, \tilde{N}^p_{Ii} = \tilde{F}^p_{ji} N_{I,j} \tag{27}$$

Some assumptions have to be made to perform time stepping. To evaluate the integral of the stress or strain at the next time step we will assume that :

$$\begin{cases} \hat{\Sigma}_{n+1} & = \hat{\Sigma}_n + dt \hat{\sigma}_{n+1} \\ \hat{E}_{n+1} & = \hat{E}_n + dt \hat{\epsilon}_{n+1} \end{cases} \tag{28}$$

Thus using this assumption, the internal forces term can be rewrite as :

$$p^e_{n+1} = \int_{\Omega_e} \tilde{B}^T \hat{\sigma}_{n+1} d\Omega_e + \int_{\Omega_e} \tilde{B}^{pT} \hat{\Sigma}_n d\Omega_e \tag{29}$$

where

$$\tilde{B}^T = \tilde{B}^{eT} + dt \tilde{B}^{pT} \tag{30}$$

An additional assumption has to be made to evaluate the derivative of the strain :

$$\dot{\epsilon}_{n+1} = \frac{\epsilon_{n+1} - \epsilon_n}{dt} \tag{31}$$

This corresponds to the first order approxiation due to Taylor's theorem. Using this assumption in the third equation of 13, the expression of the strain for the next time step can be obtained.

$$\hat{\epsilon}_{n+1} = \frac{1}{dt} \left(B^\epsilon \dot{U}_{n+1} + B^Q U_{n+1} + \frac{1}{dt} \hat{F}^\epsilon \hat{\epsilon}_n - \hat{F}^Q \hat{E}_n \right) \tag{32}$$

The matrices B^ϵ, B^Q, $\hat{F}^\epsilon$ and $\hat{F}^Q$ depend on the attenuation and the nodal shape functions. The are defined by their nodal submatrices as :

$$B^\epsilon_I = \begin{bmatrix} F^\epsilon_{11} N^I_{I1} & F^\epsilon_{21} N^I_{I1} \\ F^\epsilon_{12} N^I_{I2} & F^\epsilon_{22} N^I_{I2} \\ F^\epsilon_{11} N^I_{I2} + F^\epsilon_{12} N^I_{I1} & F^\epsilon_{21} N^I_{I2} + F^\epsilon_{22} N^I_{I1} \end{bmatrix} \tag{33}$$

with

$$N_{Ii}^{I} = F_{ij}^{I} N_{I,j} \tag{34}$$

$$F^{I} = \left[F^{p} + \frac{F^{e}}{dt} \right]^{-1}, F^{\epsilon} = F^{e} F^{I}, F^{Q} = F^{p} F^{I} \tag{35}$$

and

$$\hat{F}_{I}^{\epsilon} = \begin{bmatrix} (F_{11}^{\epsilon})^2 & (F_{21}^{\epsilon})^2 & F_{11}^{\epsilon} F_{21}^{\epsilon} \\ (F_{12}^{\epsilon})^2 & (F_{22}^{\epsilon})^2 & F_{12}^{\epsilon} F_{22}^{\epsilon} \\ 2F_{11}^{\epsilon} F_{12}^{\epsilon} & 2F_{21}^{\epsilon} F_{22}^{\epsilon} & F_{11}^{\epsilon} F_{22}^{\epsilon} + F_{12}^{\epsilon} F_{21}^{\epsilon} \end{bmatrix} \tag{36}$$

To obtain the relations for B^Q and $\hat{F}^Q$ the only thing to replace is the superscript ϵ by Q.

The stress $\hat{\sigma}_{n+1}$ is computed using the second equation of 13 involving the elastic constitutive tensor C. Thus the internal forces term can be expressed in function of the strain and not the stress.

$$p_{n+1}^{e} = \int_{\Omega_e} \tilde{B}^{T} D \hat{\epsilon}_{n+1} d\Omega_e + \int_{\Omega_e} \tilde{B}^{pT} \hat{\Sigma}_n d\Omega_e \tag{37}$$

and using the relation 32 this expression can be rewrite as :

$$p_{n+1}^{e} = \int_{\Omega_e} \tilde{B}^{T} D \left[\frac{1}{dt} \left(B^{\epsilon} \dot{U}_{n+1} + B^{Q} U_{n+1} + \frac{1}{dt} \hat{F}^{\epsilon} \hat{\epsilon}_n - \hat{F}^{Q} \hat{E}_n \right) \right] d\Omega_e + \int_{\Omega_e} \tilde{B}^{pT} \hat{\Sigma}_n d\Omega_e \tag{38}$$

$$= \tilde{c}^{e} \dot{U}_{n+1}^{e} + \tilde{k}^{e} U_{n+1}^{e} + P(\hat{\epsilon}_n, \hat{E}_n, \hat{\Sigma}_n) \tag{39}$$

where

$$P(\hat{\epsilon}_n, \hat{E}_n, \hat{\Sigma}_n) = \int_{\Omega_e} \tilde{B}^{T} \frac{D}{dt} \left[\frac{1}{dt} \hat{F}^{\epsilon} \hat{\epsilon} - \hat{F}^{Q} \hat{E}_n \right] + \tilde{B}^{p} \hat{\Sigma}_n d\Omega_e \tag{40}$$

and

$$\tilde{c}^{e} = \frac{1}{dt} \int_{\Omega_e} \tilde{B}^{T} D B^{\epsilon} d\Omega_e \tag{41}$$

$$\tilde{k}^{e} = \frac{1}{dt} \int_{\Omega_e} \tilde{B}^{T} D B^{Q} d\Omega_e \tag{42}$$

Under the plane-strain assumption the material constitutive matrix is expressed as :

$$\begin{pmatrix} K + \frac{4}{3}\mu_L & K - \frac{2}{3}\mu_L & 0 \\ K - \frac{2}{3}\mu_L & K + \frac{4}{3}\mu_L & 0 \\ 0 & 0 & \mu_L \end{pmatrix} \tag{43}$$

Therefore using the above equation we can rewrite 20 as :

$$M\ddot{U}_{n+1} + \left(C + \tilde{C} \right) \dot{U}_{n+1} + \left(K + \tilde{K} \right) U_{n+1} + P(\hat{\epsilon}_n, \hat{E}_n, \hat{\Sigma}_n) = F_{ext} \tag{44}$$

Where M,C and K are respectively the mass, damping and stiffness matrices resulting from the assembly of their element matrices 21, 22 and 23. The matrices $\tilde{K}$ and $\tilde{C}$ derive from the assembly procedure of their element matrices 42 and 41. $P(\hat{\epsilon}_n, \hat{E}_n, \hat{\Sigma}_n)$ is given by the equation 40 and is known at the beginning of the time step since it depends only on components of the previous time.

1.6 Time integration scheme

The complete discrete equations obtained in the previous part can be integrated using the Newmark-β scheme. The classical Newmark approximation formulas are expressed in acceleration form :

$$\begin{cases} U_{n+1} = U_{n,p} + \beta dt^2 \ddot{U}_{n+1} \\ \dot{U}_{n+1} = \dot{U}_{n,p} + \gamma dt \ddot{U}_{n+1} \end{cases} \tag{45}$$

where the predictors $U_{n,p}$ and $\dot{U}_{n,p}$ have the form :

$$\begin{cases} U_{n,p} = U_n + dt\dot{U}_n + dt^2 \left(\frac{1}{2} - \beta\right) \ddot{U}_n \\ \dot{U}_{n,p} = \dot{U}_n + dt(1-\gamma)\ddot{U}_n \end{cases} \tag{46}$$

Substituting the equations 45 and 46 into the discrete form of the equation of motion 44 the acceleration at time t_{n+1} can be obtained.

$$\tilde{M}\ddot{U}_{n+1} = F_{ext} - \left(C + \tilde{C}\right)\dot{U}_{n,p} - \left(K + \tilde{K}\right)U_{n,p} - P(\hat{\epsilon}_n, \hat{E}_n, \hat{\Sigma}_n) \tag{47}$$

where

$$\tilde{M} = M + \gamma dt \left(C + \tilde{C}\right) + \beta dt^2 \left(K + \tilde{K}\right) \tag{48}$$

This matrix needs to be inverted, this will be done before beginning the time stepping since all the matrices constituting it remain constant through the time stepping. Two schemes will be used in the following of this report :

— Implicit Newmark scheme : with $\gamma = 1/2$ and $\beta = 1/4$.

— Explicit Newmark scheme : with $\gamma = 1/2$ and $\beta = 0$.

The properties of each scheme will be investigated in the next section concerning the stability and the last part will highlight the differences in term of performance and accuracy.

Let us summarise the different steps in the following algorithm :

Algorithm 1 PML algorithm

Require: Calculate global matrices : M, C, K.

Require: Calculate : $\tilde{M}^{-1} = \left[M + \gamma h C + \beta h^2 K\right]^{-1}$

Require: Calculate constant matrices to update internal forces for PML.

while not end time **do**

for each element **do**

$P(\hat{\epsilon}_n, \hat{E}_n, \hat{\Sigma}_n) = \sum_{gp} \tilde{B}^T \frac{D}{dt} \left[\frac{1}{dt}\hat{F}^{\epsilon}\hat{\epsilon} - \hat{F}^{Q}\hat{E}_n\right] + \tilde{B}^p \hat{\Sigma}_n$

end for

Compute the external forces : $F_{ext,n+1}$

$u_{n+1,p} \leftarrow u_n + h\dot{u}_n + h^2(\frac{1}{2} - \beta)\ddot{u}_n$

$\dot{u}_{n+1,p} \leftarrow \dot{u}_n + h(1-\gamma)\ddot{u}_n$

$\ddot{u}_{n+1} \leftarrow \tilde{M}^{-1}\left(P(\hat{\epsilon}_n, \hat{E}_n, \hat{\Sigma}_n) - C\dot{u}_{n+1,p} - K u_{n+1,p}\right)$

$u_{n+1} \leftarrow u_{n+1,p} + h^2\beta\ddot{u}_{n+1}$

$\dot{u}_{n+1} \leftarrow \dot{u}_{n+1,p} + h\gamma\ddot{u}_{n+1}$

Update physical quantities : ϵ_{n+1}, E_{n+1}, σ_{n+1} and Σ_{n+1}

$t \leftarrow t + h$

end while

2 Stability of the numerical method

2.1 Description

2.1.1 Principle

In order to prove the stability of the temporal scheme, we can recall the following result concerning integration methods [23] : An integration scheme is said to be stable if there exists an integration step $h_0 > 0$ so that for any $h \in [0, h_0]$, a finite variation of the state vector at time t^n induces only a non-increasing variation of the state vector X^{n+1} calculated at a subsequent instant t^{n+1}.
In our case we will study the stability of the scheme with the temporal discretization presented in the previous section. We will focus our attention on the stability of the temporal scheme applied on only one element. If we can prove the stability on one element, the result extends to the others [32].
Therefore, if we define 2 initial states : a non-perturbed X_0 and a perturbed X'_0 one. We can define the initial disturbance :

$$\delta X_0 = X'_0 - X_0 \tag{49}$$

The state vector of the non-perturbed solution is defined in function of the amplification matrix H :

$$\begin{aligned} X_{n+1} &= HX_n + g_{n+1} && (50)\\ &= H^2 X_{n-1} + Hg_n + g_{n+1} && (51)\\ &\vdots && (52)\\ &= H^{n+1}X_0 + \sum_{j=0}^{n+1} H^{n-j+1} g_j && (53) \end{aligned}$$

This formulation permits to express the state vector at a time t_{n+1} in function of the amplification matrix and the initial solution X_0. The perturbed solution can be expressed in the same manner :

$$X'_{n+1} = H^{n+1}X'_0 + \sum_{j=0}^{n+1} H^{n-j+1} g_j \tag{54}$$

Therefore the effect of the disturbance can be expressed at the time t_{n+1} by subtracting 54 to 53 :

$$\delta X_{n+1} = H^{n+1}\delta X_0 \tag{55}$$

The resulting eigenvalue problem is defined by :

$$det(H - \lambda I) = 0 \tag{56}$$

We can define $\lambda_r, x_{(r)}$ the associated eigenvalues and eigenvectors of the amplification matrix. The initial disturbance can be expressed as a combination of the eigenvectors :

$$\delta X_0 = \sum_{s=1}^{2N} a_s x_{(s)} \tag{57}$$

The recurrence relationship for the disturbance can be changed using 57 to obtain :

$$\begin{aligned} \delta X_{n+1} &= H^{n+1} \sum_{s=1}^{2N} a_s x_{(s)} && (58)\\ &= \sum_{s=1}^{2N} a_s \lambda_s^{n+1} x_{(s)} && (59) \end{aligned}$$

Using this formulation we can observe that the disturbance will be amplified if the moduli of the eigenvalues of the amplification matrix are higher than 1. In order to maintain the stability of a numerical scheme the spectral radius of the eigenvalues has to remain below 1.

To apply this method to our PML scheme, described by the equations 46 and 44, we have to construct the amplification matrix. We seek a system of equation such as :

$$A(h)X_{n+1} + B(h)X_n = 0 \tag{60}$$

And the amplification matrix H will be defined as :

$$X_{n+1} = -A^{-1}B(h)X_n = HX_n \tag{61}$$

2.1.2 Definitions of the stability criterion

To obtain the proof of the stability of the integration scheme associated with the PML and to have some insights about its accuracy we have to define the different parameters that will be calculated and analysed.
First of all to prove the stability of the scheme we will calculate the eigenvalues of the amplification matrix. By representing them in the complex plane and by calculating the spectral radius we will conclude about the stability. In fact, only the spectral radius can lead to a conclusion about the stability of a scheme, but in the analysis of the results all moduli of all eigenvalues will be represented. This will allow us to see clearly the evolution of the different eigenvalues separately in function of the time step h.
The spectral radius is defined by :

$$\rho(H(h)) = \max_i |\lambda_i| \tag{62}$$

If the scheme is unconditionally stable the spectral radius over all the values of time step has to remain below the value 1 and the representation of the eigenvalues in the complex space will remain within the unit circle. If the scheme is conditionally stable, we will be able to define the limit of stability, i.e. the time step for which the spectral radius is larger than 1.
To be able to analyse the accuracy of the scheme, we will use two parameters : the numerical damping $\bar{\epsilon}$ and the relative periodicity error $\frac{\Delta T}{T}$. The numerical damping is a measure of the amplitude error and is defined for the time step h and the eigenvalue λ_i by :

$$\bar{\epsilon}\omega h = -\frac{1}{2}\log(|\lambda_i|) \tag{63}$$

and the relative periodicity error by :

$$\frac{\Delta T}{T} = \frac{\omega_i}{\overline{\omega_i}} - 1 \tag{64}$$

2.1.3 Material parameters and time integration scheme

We will consider in the following of this section a simple bilinear quadrilateral element with the following material parameters :

Table 2 – Material parameters for an element of the elastic medium

ν	0.24
E	$1e07$
ρ	1700
a	1
b	1

Where a and b correspond to the length and the height of the element. For the standard medium element only these parameters will be used. For the PML element we have to add the attenuation and we will consider it constant along the element. We will evaluate the impact of f_p and f_e for different values of attenuation.
We will analyse the stability of two time integration schemes : Newmark implicit which is known to be unconditionally stable for the standard element and Newmark explicit which is known to be conditionally stable.

2.2 Construction of the amplification matrix

In this version of the construction of the amplification matrix for the numerical scheme related to the two-dimensional perfectly matched layer, the state vectors at time t_{n+1} and t_n will have the following form :

$$X_n = \begin{pmatrix} \dot{u}_n \\ u_n \\ \hat{\epsilon}_n \\ \hat{\Sigma}_n \\ \hat{E}_n \end{pmatrix}, \qquad X_{n+1} = \begin{pmatrix} \dot{u}_{n+1} \\ u_{n+1} \\ \hat{\epsilon}_{n+1} \\ \hat{\Sigma}_{n+1} \\ \hat{E}_{n+1} \end{pmatrix} \tag{65}$$

Let us state the equations of motion for time t_{n+1} and t_n :

$$M\ddot{u}_{n+1} + C\dot{u}_{n+1} + Ku_{n+1} + p^e_{n+1} = F_{ext} \tag{66}$$

$$M\ddot{u}_n + C\dot{u}_n + Ku_n + p^e_n = F_{ext} \tag{67}$$

With

$$p^e_{n+1} = \int_{\Omega_e} \tilde{B}^{eT} \hat{\sigma}_{n+1} d\Omega_e + \int_{\Omega_e} \tilde{B}^{pT} \hat{\Sigma}_{n+1} d\Omega_e \tag{68}$$

We will also use the recurence relationships given by the Newmark-β method.

$$\begin{cases} u_{n+1} = u_n + \Delta t \dot{u}_n + \Delta t^2 \left(\frac{1}{2} - \beta\right) \ddot{u}_n + \beta \Delta t^2 \ddot{u}_{n+1} \\ \dot{u}_{n+1} = \dot{u}_n + \Delta t(1-\gamma)\ddot{u}_n + \gamma \Delta t \ddot{u}_{n+1} \end{cases} \tag{69}$$

Multiplying these relations 69 by the mass matrix M and using 66, 67, we obtain :

$$\begin{cases} Mu_{n+1} = Mu_n + \Delta t M\dot{u}_n + \Delta t^2 \left(\frac{1}{2} - \beta\right) \left[-C\dot{u}_n - Ku_n - p^e_n\right] + \beta \Delta t^2 \left[-C\dot{u}_{n+1} - Ku_{n+1} - p^e_{n+1}\right] \\ M\dot{u}_{n+1} = M\dot{u}_n + \Delta t(1-\gamma) \left[-C\dot{u}_n - Ku_n - p^e_n\right] + \gamma \Delta t \left[-C\dot{u}_{n+1} - Ku_{n+1} - p^e_{n+1}\right] \end{cases} \tag{70}$$

Let us express these relations as :

$$\begin{cases} Mu_{n+1} - Mu_n - \Delta t M\dot{u}_n - \Delta t^2 \left(\frac{1}{2} - \beta\right) \left[-C\dot{u}_n - Ku_n - p^e_n\right] - \beta \Delta t^2 \left[-C\dot{u}_{n+1} - Ku_{n+1} - p^e_{n+1}\right] = 0 \\ M\dot{u}_{n+1} - M\dot{u}_n - \Delta t(1-\gamma) \left[-C\dot{u}_n - Ku_n - p^e_n\right] - \gamma \Delta t \left[-C\dot{u}_{n+1} - Ku_{n+1} - p^e_{n+1}\right] = 0 \end{cases} \tag{71}$$

The integral in the expression of the internal forces p^e_{n+1} needs to be evaluated. We will use Gaussian quadrature to express this integral :

$$p^e_{n+1} = \sum_i \sum_j \tilde{B}^{eT}(\xi_i, \eta_j) \hat{\sigma}_{n+1}(\xi_i, \eta_j) + \tilde{B}^{pT}(\xi_i, \eta_j) \hat{\Sigma}_{n+1}(\xi_i, \eta_j) = M^{\tilde{B}^e} \hat{\sigma}_{n+1} + M^{\tilde{B}^p} \hat{\Sigma}_{n+1} \tag{72}$$

This sum is expressed in matrix form using the matrices :

$$M^{\tilde{B}^e} = [\tilde{B}^{eT}(\xi_1, \eta_1) \tilde{B}^{eT}(\xi_1, \eta_2) ... \tilde{B}^{eT}(\xi_{ng}, \eta_{ng})] \tag{73}$$

$$M^{\tilde{B}^p} = [\tilde{B}^{pT}(\xi_1,\eta_1)\tilde{B}^{pT}(\xi_1,\eta_2)...\tilde{B}^{pT}(\xi_{ng},\eta_{ng})] \tag{74}$$

Thus the relations 71 are rewritten as :

$$Mu_{n+1} - Mu_n - \Delta t M\dot{u}_n - \Delta t^2\left(\frac{1}{2}-\beta\right)\left[-C\dot{u}_n - Ku_n - M^{\tilde{B}^e}\hat{\sigma}_n - M^{\tilde{B}^p}\hat{\Sigma}_n\right] \tag{75}$$

$$-\beta\Delta t^2\left[-C\dot{u}_{n+1} - Ku_{n+1} - M^{\tilde{B}^e}\hat{\sigma}_{n+1} - M^{\tilde{B}^p}\hat{\Sigma}_{n+1}\right] = 0 \tag{76}$$

$$M\dot{u}_{n+1} - M\dot{u}_n - \Delta t(1-\gamma)\left[-C\dot{u}_n - Ku_n - M^{\tilde{B}^e}\hat{\sigma}_n - M^{\tilde{B}^p}\hat{\Sigma}_n\right] \tag{77}$$

$$-\gamma\Delta t\left[-C\dot{u}_{n+1} - Ku_{n+1} - M^{\tilde{B}^e}\hat{\sigma}_{n+1} - M^{\tilde{B}^p}\hat{\Sigma}_{n+1}\right] = 0 \tag{78}$$

For the stress, we also have the constitutive relationship :

$$\hat{\sigma}_{n+1} = D\hat{\epsilon}_{n+1} \tag{79}$$

And the following assumptions :

$$\begin{cases} \dot{\epsilon}_{n+1} = \frac{\epsilon_{n+1}-\epsilon_n}{\Delta t} \\ E_{n+1} = E_n + \Delta t\epsilon_{n+1} \\ \Sigma_{n+1} = \Sigma + \Delta t\sigma_{n+1} \end{cases} \tag{80}$$

Using the first assumption in the third equation of 13 we obtain the following relation :

$$\hat{\epsilon}_{n+1} = \frac{1}{dt}\left(B^{\epsilon}\dot{U}_{n+1} + B^{Q}U_{n+1} + \frac{1}{dt}\hat{F}^{\epsilon}\hat{\epsilon}_n - \hat{F}^{Q}\hat{E}_n\right) \tag{81}$$

Using the above relations we can construct our amplification matrix from the following matrices A and B.

$$A = \begin{bmatrix} I_d + dt\gamma M^{-1}C & dt\gamma M^{-1}K & dt\gamma M^{-1}M^{\tilde{B}^e}M^D & dt\gamma M^{-1}M^{\tilde{B}^p} & 0 \\ dt^2\beta M^{-1}C & Id + dt^2\beta M^{-1}K & dt^2\beta M^{-1}M^{\tilde{B}^e}M^D & dt^2\beta M^{-1}M^{\tilde{B}^p} & 0 \\ 0 & 0 & -M^D & Id & 0 \\ -\frac{1}{dt}M^{B^{\epsilon}} & -\frac{1}{dt}M^{B^Q} & I_d & 0 & 0 \\ 0 & 0 & -dtI_d & 0 & I_d \end{bmatrix} \tag{82}$$

In this matrix A, on the fourth "row", the matrix M^D is a squared matrix such that on the diagonal we have blocs of size 3×3 correspnding to the matrix D. Here the identity matrix I_d is of size $3*(ng^2)\times 3*(ng^2)$. We also have the definition of the matrix B.

$$B = \begin{bmatrix} -I_d + dt(1-\gamma)M^{-1}C & dt(1-\gamma)M^{-1}K & dt(1-\gamma)M^{-1}M^{\tilde{B}^e}M^D & dt(1-\gamma)M^{-1}M^{\tilde{B}^p} & 0 \\ -dtI_d + dt^2(\frac{1}{2}-\beta)M^{-1}C & -Id + dt^2(\frac{1}{2}-\beta)M^{-1}K & dt^2(\frac{1}{2}-\beta)M^{-1}M^{\tilde{B}^e}M^D & dt^2(\frac{1}{2}-\beta)M^{-1}M^{\tilde{B}^p} & 0 \\ 0 & 0 & 0 & -I_d & 0 \\ 0 & 0 & -\frac{1}{dt^2}\hat{F}^{\epsilon} & 0 & \frac{1}{dt}\hat{F}^{Q} \\ 0 & 0 & 0 & 0 & -I_d \end{bmatrix} \tag{83}$$

2.3 Stability results

2.3.1 Generic bilinear quadrilateral element

To analyse the results for the numerical stability concerning the PML we will review the results obtained on a simple linear 4-noded element (figure 2).

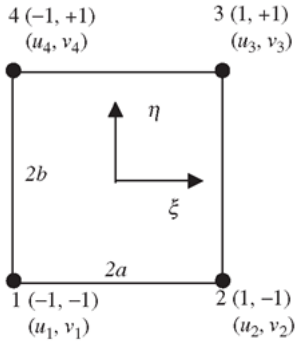

FIGURE 2 – Generic bilinear quadrilateral element

The numerical scheme used and the construction of the amplification matrix for this element can be found in [23] : it follows the same steps as the construction presented in the case of the 2D PML. The resulting amplification matrix has a size of 8×8. The analysis of the amplification matrix is closely related to the study of the normal modes of deformation of the element. In fact, the eigenvectors of the amplification matrix represent the natural modes and the eigenvalues are the natural frequencies of the deformation associated. For a standard bilinear 4-noded element the natural modes of deformation are represented in the following figure borrowed from [37].

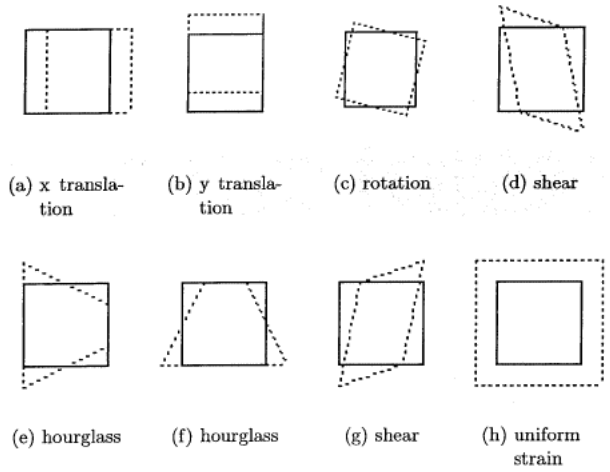

FIGURE 3 – Deformation modes corresponding to the eigenmodes on a bilinear quadrilateral element

One of these deformation modes is dominant over the other and correspond to ω_{max} which is the maximum frequency over all the deformation modes. According to [37], this dominant mode is different in function of the Poisson's ratio. In fact, below a certain transition value the dominant mode is either shear-mode or hourglass mode of deformation depending on the formulation. Above this transition value the uniform normal strain mode dominates.

— Implicit scheme : To validate our method let us test it on the Implicit Newmark scheme applied on the discretisation of the equations of motion of the elastic medium. We obtain for several values of time step h taken within the interval $[0.0001, 0.1]$ by steps of 0.0001. ω_{max} is taken to be the frequency of the shear mode of deformation. For each value of time step we calculate the amplification matrix and its eigenvalues. We obtain the following representation in the complex plane of the eigenvalues and the spectral radius. For each time step we obtain 8 eigenvalues since the amplification matrix is of size 8×8.

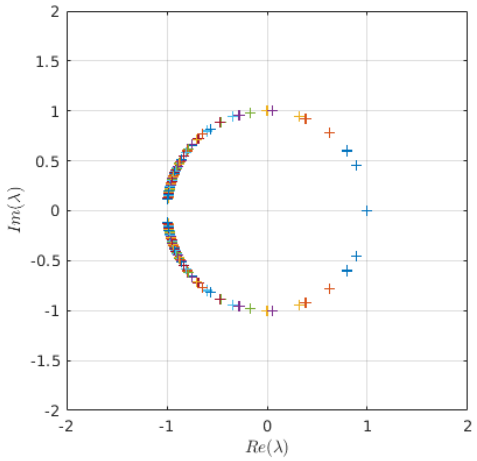

FIGURE 4 – Eigenvalues of the amplification matrix in complex plane

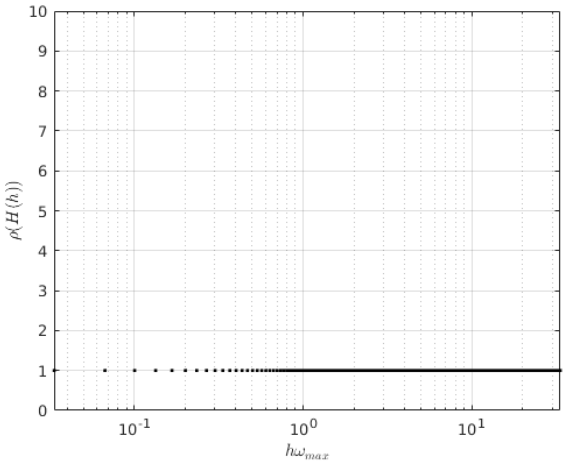

FIGURE 5 – Spectral radius of the amplification matrix

As we expected the scheme is stable : this can be observed by looking at the figures 4 and 5. The representation of the eigenvalues remains in the unit circle and the spectral radius remains below 1 for all values of the time step.

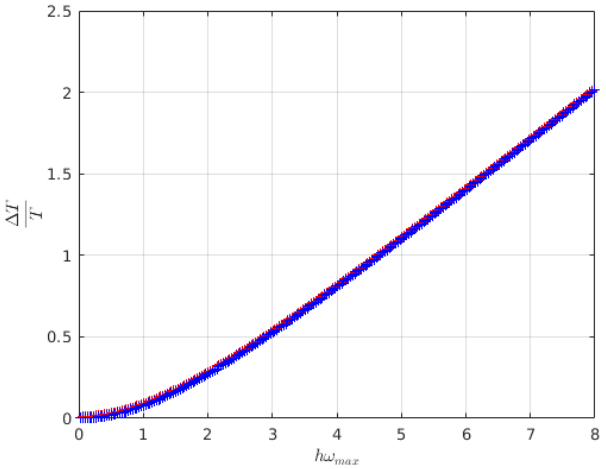

FIGURE 6 – Relative periodicity error

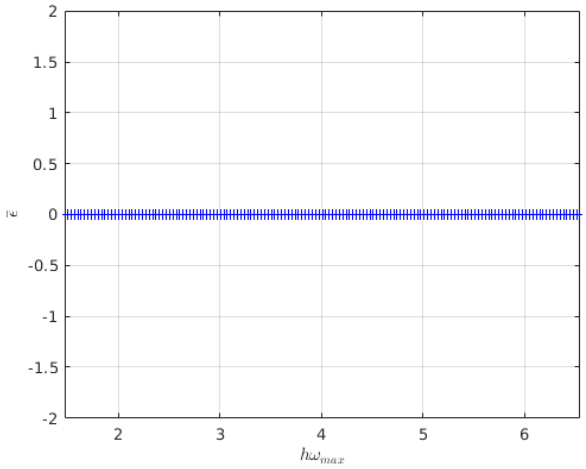

FIGURE 7 – Numerical damping ratio

As we expected the error in term of period increases with the time step (fig. 6). The more the time step increases the more the error committed by the scheme is important. The numerical damping

ratio remains equal to 0 because the Newmark implicit scheme is known to not add any artificial damping.

— Explicit Newmark scheme : The same method with the same values of the time step is used here. We obtained the following results :

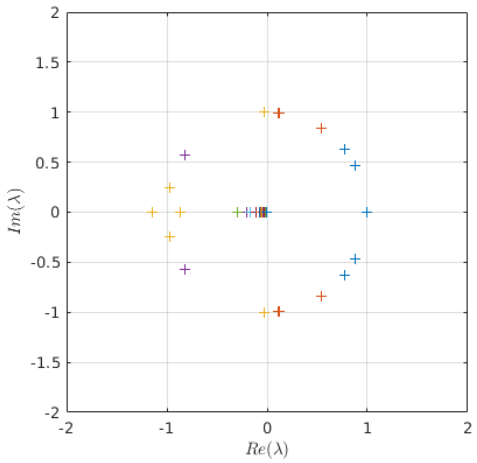

FIGURE 8 – Eigenvalues of the amplification matrix in complex plane

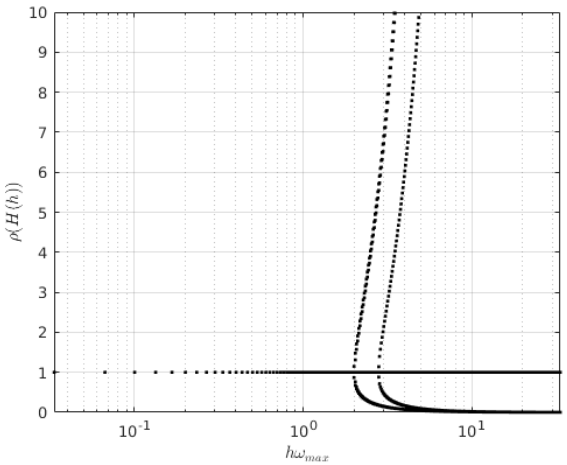

FIGURE 9 – Spectral radius of the amplification matrix

The Newmark explicit scheme is known to be conditionally stable, which means that above a certain value of the time step the scheme becomes unstable. This situation appears on the figures 8 where the eigenvalues for a certain time step go out of the unit circle and 9 on which we can observe that the spectral radius of the amplification matrix is above 1 after a critical value of time step. In the literature [23], we can find that the critical value is $\omega_{max}h = 2$. Let us make a zoom of the figure 9 :

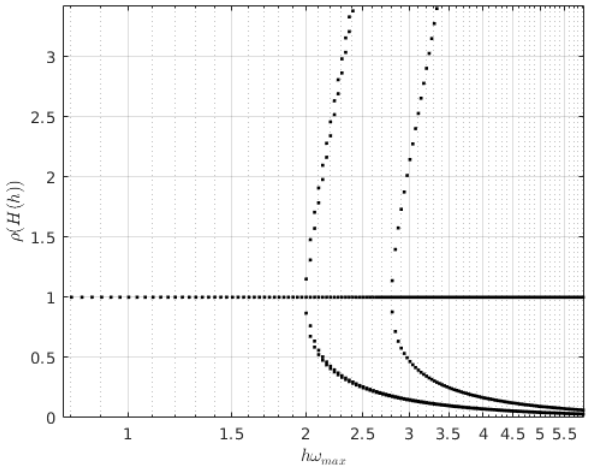

FIGURE 10 – radius of the amplification matrix

We can observe that the scheme becomes unstable for the same value of critical $\omega_{max}h$ than in the literature.

Since the integration scheme is unstable, the analysis of the numerical damping ratio and the relative periodicity error is meaningless because their values will be absurd as you can see on the figures 11 and 12.

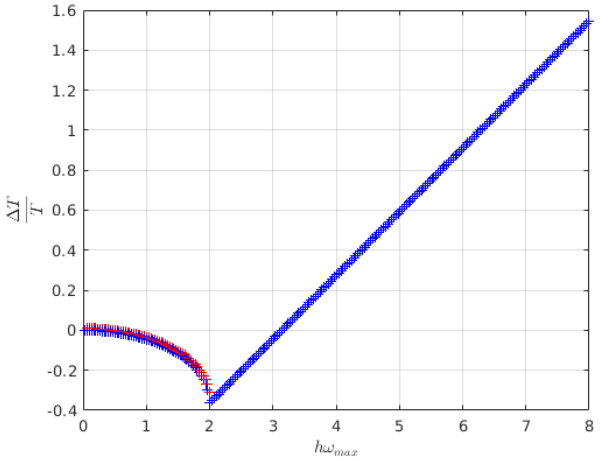

FIGURE 11 – Relative periodicity error

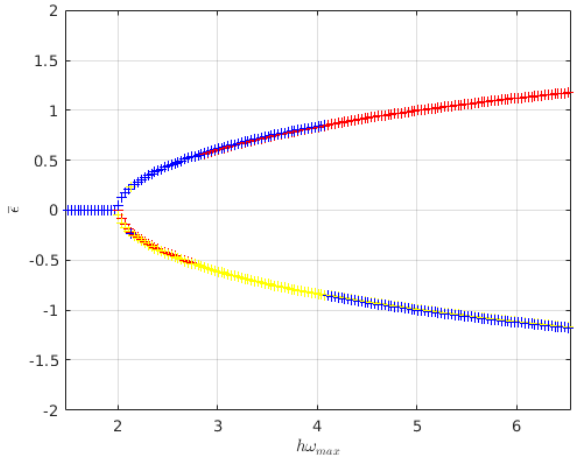

FIGURE 12 – Numerical damping ratio

We can only observe that when the scheme is stable, the relative periodicity error is negative. This result is not surprising since explicit schemes are known to introduce a negative error in terms of period.

2.3.2 PML element

Using the previous results we can conclude that our method is able to retrieve the proof of the stability of the Newmark integration scheme associated with the discrete equations of motion of an elastic medium. Let us now review the results obtained with the same integration schemes : Explicit and Implicit Newmark on a PML element.

— Implicit Newmark scheme : Let us calculate the eigenvalues of the amplification matrix associated with the PML for values of the time step h taken in the interval $[1e-3, 1]$ with a step of $1e-3$. The frequency ω_{max} is taken to be the frequency of the shear mode of deformation of the element without the PML. The attenuation is supposed to be constant along the element. Therefore, the functions $f_e(x)$ and $f_p(x)$ are equal to 10 and are constant along the element. On the two following figures, we will represent all the eigenvalues in the complex plane and their modulus for each time step.

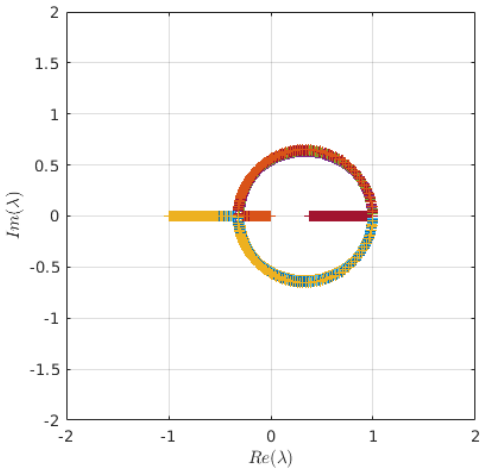

FIGURE 13 – eigenvalues in the complex plane

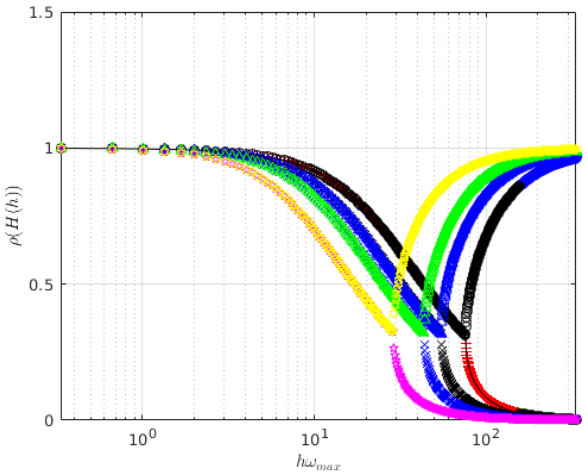

FIGURE 14 – Moduli of the eigenvalues

By analizing the two figures 13 and 14, we can observe that the implicit scheme associated with the pml is unconditionally stable since the eigenvalues remain in the unit circle. They are not precisely on it because the attenuation in the element decreases the amplitude of the deformation. As we can see on the figure 14 the moduli of the eigenvalues decrease and this decay starts at a certain frequency.
By increasing the attenuation in the element, another property of the PML can be shown. Let us consider $f_p = f_e = 100$ and reproduce the same figures.

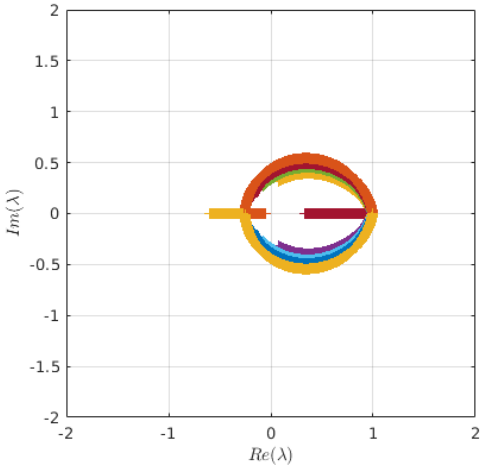

FIGURE 15 – eigenvalues in the complex plane

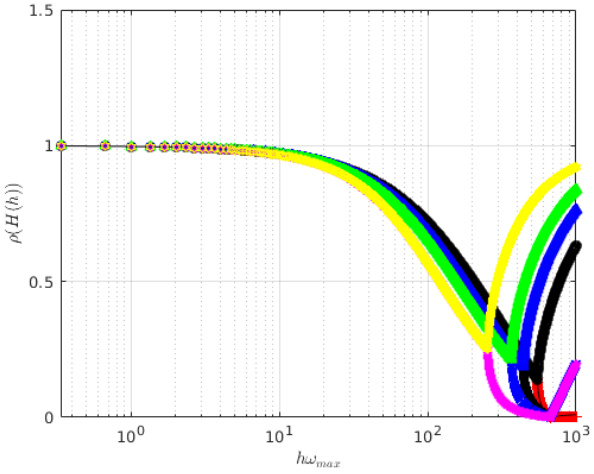

FIGURE 16 – Moduli of the eigenvalues

Comparing the figures 13 and 15, we can observe that the circles formed by the representation of the eigenvalues is flatter when the attenuation is stronger. We can conclude that the attenuation of all modes of deformation is stronger when we increase the attenuation. By comparing the figures 14 and 16 we can observe that the range of frequencies attenuated by the PML becomes larger when we increase the attenuation. This result highlights a property of the PML : we can attenuate waves of all frequencies by a careful choice of the parameter of the PML. Also, we can observe that choosing a higher value of attenuation leads to the ability of the PML to attenuate higher

frequencies.
Let us now review the results concerning the relative periodicity error and the numerical damping ratio. We pick again the value of attenuation $f_p = f_e = 10$. An important observation with the formulation of the amplification matrix is that it leads to the calculation of eigenvalues and eigenmodes of deformation not related to any "physical" mode of deformation. This is of course due to the fact that the PML is not a physical material, its only purpose is to attenuate wave and this leads to the presence of spurious modes. Their values of relative periodicity error and numerical damping ratio are not to be considered and are in fact aberrant. The main thing that we already reviewed is, for the implicit scheme, they do not lead to the instability of the scheme. We will consider in this part, the analysis of the results for the dominant mode of deformation, the shear mode.

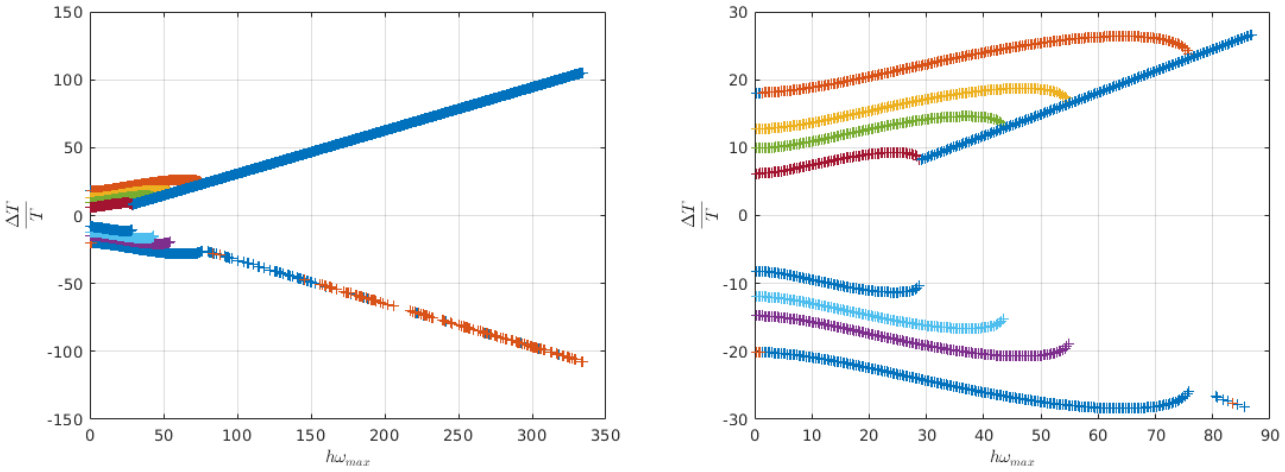

FIGURE 17 – Relative periodicity error

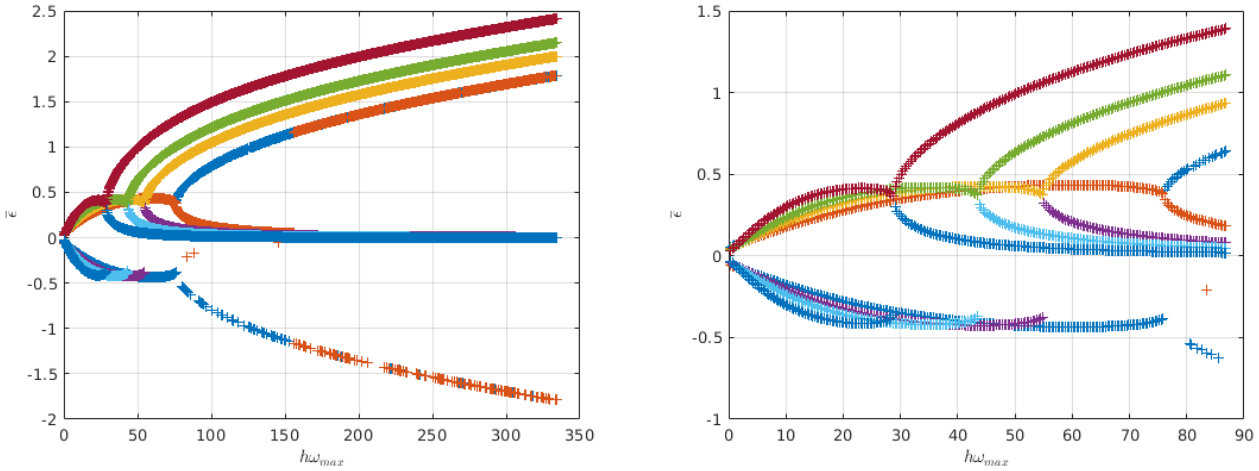

FIGURE 18 – Numerical damping ratio

It is difficult to analyse precisely the results of the relative periodicity error shown on the figure 17. The PML is not a physical medium and the error in period is not important since its purpose is to

attenuate the wave and not propagating it. Therefore the error in period is not too important and it increases with larger values of the time step which is a common result for numerical simulation schemes. The PML is conceived to introduce an artificial damping in the system, this is why we can observe on the figure 18 that, even the implicit Newmark scheme associated with the PML introduce a numerical damping. This attenuation increases with the frequency of the wave. Of course by increasing the attenuation in the element the numerical damping ratio will take bigger values.

— Explicit Newmark scheme : We have shown in the previous part concerning the standard element stability analysis that the Explicit scheme is conditionally stable and the critical value $\omega h = 2$. Therefore, for the stability analysis of the same scheme associated with the PML we will dedicate a specific attention to the critical value where the scheme starts to become unstable. For $f_p = f_e = 10$, we obtain the following results :

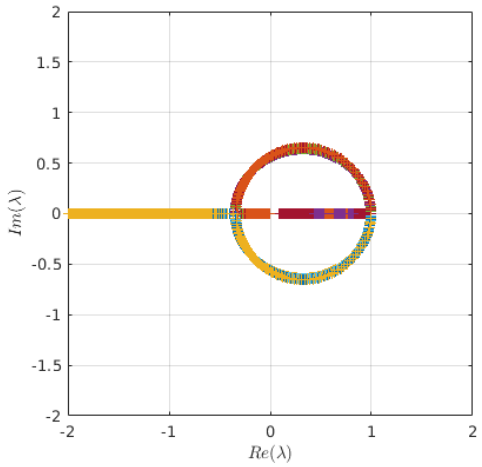

FIGURE 19 – Eigenvalues of the amplification matrix in complex plane

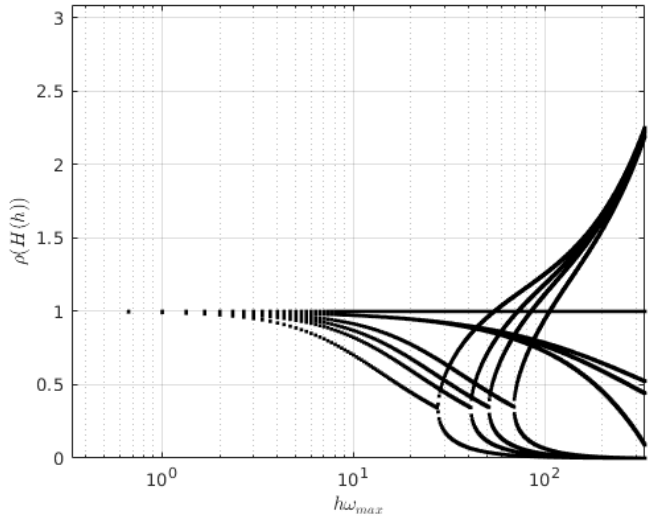

FIGURE 20 – Spectral radius

The stability of the explicit scheme associated with the PML is also conditionally stable because, as we can observe on the figure 19, the representation of the eigenvalues in the complex plane goes out the unit circle from a certain value of $\omega_{max}h$. Looking at the figure 20, we can determine this limit of stability. We can find that the critical value is $\omega_{max}h = 80$ which is of course larger than the limit of the stability of the explicit scheme associated with the standard element. Therefore we can ask ourselves why the limit of stability is extended. Some features of the PML must impact the scheme in this manner. Let us focus on the attenuation and increase the value to $f_p = f_e = 100$.

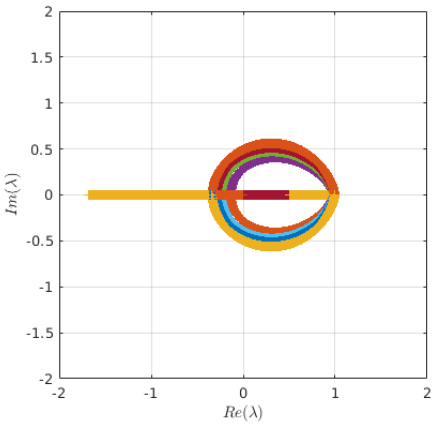

FIGURE 21 – Eigenvalues of the amplification matrix in complex plane

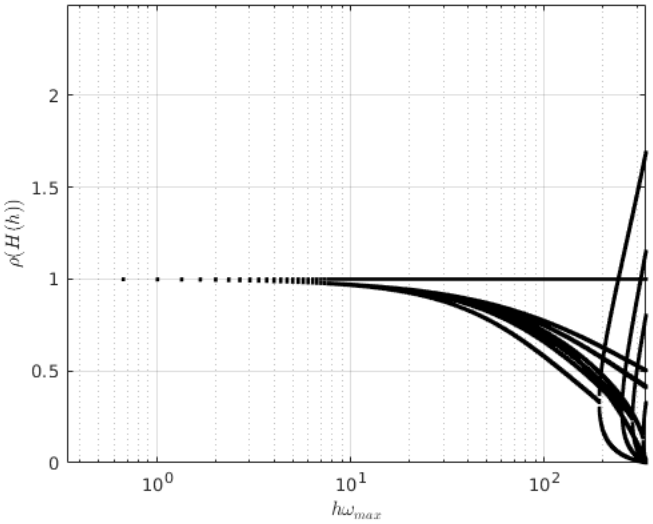

FIGURE 22 – Spectral radius

The first observation that can be made using the figure 21 is the same as in the context of the implicit scheme : increasing the attenuation makes the representation of the circle formed by the eigenvalues flatter. This is due to the fact that the amplitude of the deformation is attenuated in a stronger manner when the attenuation coefficient is larger. Secondly, using the figure 22, we can observe that by increasing the attenuation the critical value where the scheme becomes unstable is postponed to $\omega_{max}h = 200$. We can conclude that the attenuation impacts the explicit scheme and permits to take larger value of the time step while keeping the stability. An hypothesis to explain this observation is that the attenuation affects the amplitude of the deformation and therefore, is able to decay a finite variation of the state vector. This results in postponing the critical value of the time step for which this finite variation becomes too large to not introduce a non-increasing variation of the state vector at a subsequent time.
Since the scheme becomes unstable at a certain value of time step the analysis of the relative periodicity error and of the numerical damping ratio is difficult. Let us review the result using only the shear mode of deformation since it is the dominant one. We will look at the results obtained when the scheme remains stable $h < h_{crit}$. After this value the results can not be analysed since the values become too large.

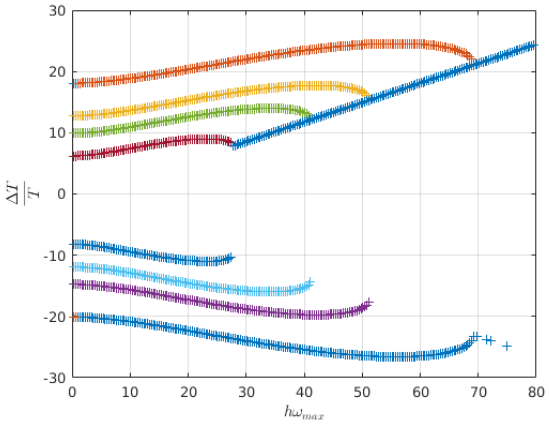

FIGURE 23 – Relative periodicity error

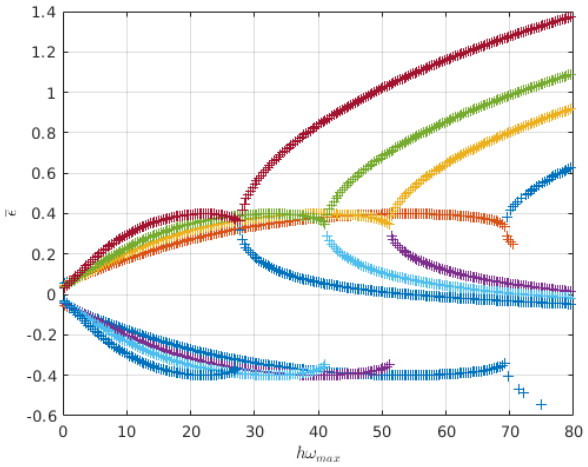

FIGURE 24 – Numerical damping ratio

Comparing to the figures 17 and 18 the results obtained in the stable part of the explicit scheme follows the same trends. Therefore the same observation can be made. The periodicity error, shown on the figure 23 is difficult to analyse. We can observe that the conjugated eigenvalues separate : one shows a positive periodicity error and the other one a negative. We can also clearly distinguish the 2 shear modes of deformation and the 2 hourglass modes. As the time step increases, they seem to meet in the same linear curve. After this joining we can not observe separately the eigenvalues correpsonding to different shear and hourglass modes. A close observation can be made about the numerical damping ratio using the figure 24. Here the numerical damping ratios obtained using the different eigenvalues associated with shear and hourglass modes do not seem to converge to a common curve. In fact at the beginning we can clearly identify the 2 shear modes and the 2 hourglass modes of deformation. The numerical damping ratio is positive and it corresponds to the attenuation present in the element. At a certain value of time step (different for each shear and hourglass mode of deformation), a separation can be observed for the numerical damping ratio associated with conjugated eigenvalues. The lower branches tend to 0 whereas the upper ones do not seem to converge to a certain value. The slope of the evolution of numerical damping for the upper branches seems to become weaker as the time step increases.

3 Numerical results

3.1 Bar test case

3.1.1 Description

The bar test case is composed of two parts and it is mainly summarized by the figure 25.

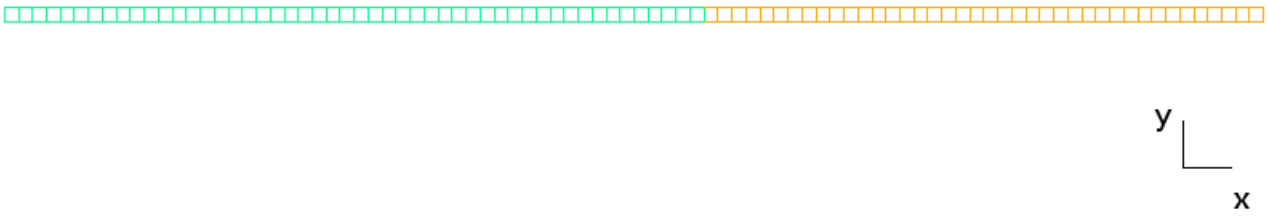

FIGURE 25 – bar with the medium (left) and the PML (right)

This test case corresponds to a simple bar with on the left an elastic medium of a length of 250 and on the right a PML with a length of 200. The size of an element is 5, thus the elastic medium contains 50 elements whereas the PML 40. The parameters of the medium are the following and they are the same for the PML.

TABLE 3 – Material parameters for the elastic medium

ν	0.24
E	$1e07$
ρ	1700

In order to calculate the coefficients of attenuation a_0 (for propagating waves) and b_0 (for evanescent waves) in both directions, we will use the formulation 8 with the reflection wanted at the end of the PML $R_{pp} = 1e-3$. The order of the attenuation functions is $n = 2$.

3.1.2 Non-harmonic input wave

In the context of the analysis of seismic data, the Ricker wave is often used. It is the normalized negative of the second derivative of a Gaussian function and takes the formulation at the point x ant time t :

$$F(x,t) = A\left(2\pi^2\frac{(t-t_s)}{t_p^2} - 1\right)\exp\left(-\pi^2\frac{(t-t_s)}{t_p^2}\right) \tag{84}$$

With t_s the time shift, t_p the fundamental period and A the amplitude. In terms of displacement this wave has the following "Mexican hat" form :

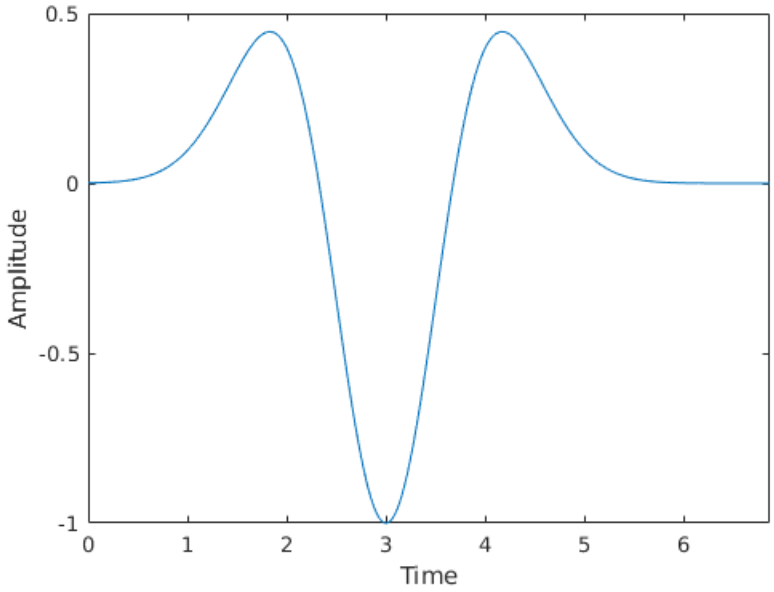

FIGURE 26 – Ricker wave in time domain

We will inject this wave at the left extremity of the medium and fix its propagation within the x direction. We will choose the set of parameter $t_p = 3$, $t_s = 3$ and $A = 1e6$ which gives us exactly the wave shown in figure 26.

3.1.3 Analysis of the results

We will use the Implicit Newmark scheme as integration scheme. The analysis of the performance will not be reviewed since it is a very simple test case. Therefore a comparison between the results obtained with the Explicit scheme is not needed. Both schemes are able to be accurate and efficient on a simple case like the bar test. For more complex cases, it will be interesting to compare the scheme and highlights the pros and cons of both schemes. For our analysis, a specific attention will be dedicated to the reflexion of the wave due to the interface. The time step used is $dt = 0.025$. For this test case the critical time step is 0.06.

Let us record the displacement of a node placed at the center of the elastic medium in both directions. On the following figures of displacement, the abscissa is the index of the time step denoted by n and in ordinate we have the displacement along the direction x for the left figures and y for the right figure.

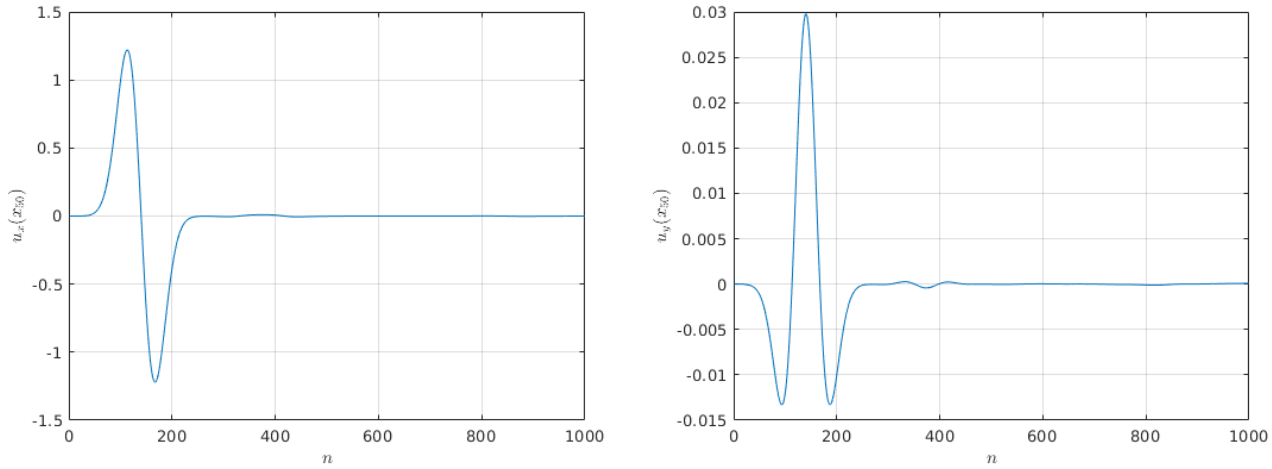

FIGURE 27 – Displacement within the x direction (left) and y direction (right)

To understand the results shown in figure 27, an explanation step by step of what is happening is necessary :

- Time steps : $[0 - 300]$ The node records the displacement due to the propagation of the wave in the elastic medium.
- Time steps : $[300 - 500]$ A very slight reflection can be observed due to the truncation interface. The node records this very small displacement because the reflected wave comes back toward the elastic medium. This wave will bounce back at the left extremity of the medium and will propagate again in the direction of the PML.
- Time steps : $[500 - 1000]$ The reflected wave encounters the truncation interface. On this figure the reflection at the point is negligible and we can consider that the wave is fully attenuated.

Of course, this reflexion due to the truncation interface is a key element of the simulation since the perfectly matched layer is designed to be able to minimize it. A simple ratio between the maximum of the initially propagated wave and the reflected one gives 0.0081. Therefore, less than 1% of the wave is reflected by the interface. Of course taking a smaller value of the time step and size of an element will decrease this percentage of the reflected wave. We have seen in the stability analysis that the implicit scheme commits an error that evolves with the time step considered.
The analysis of the energies of the system is important since the PML has the faculty of attenuate waves, it has also the power of decaying the energies in the system.

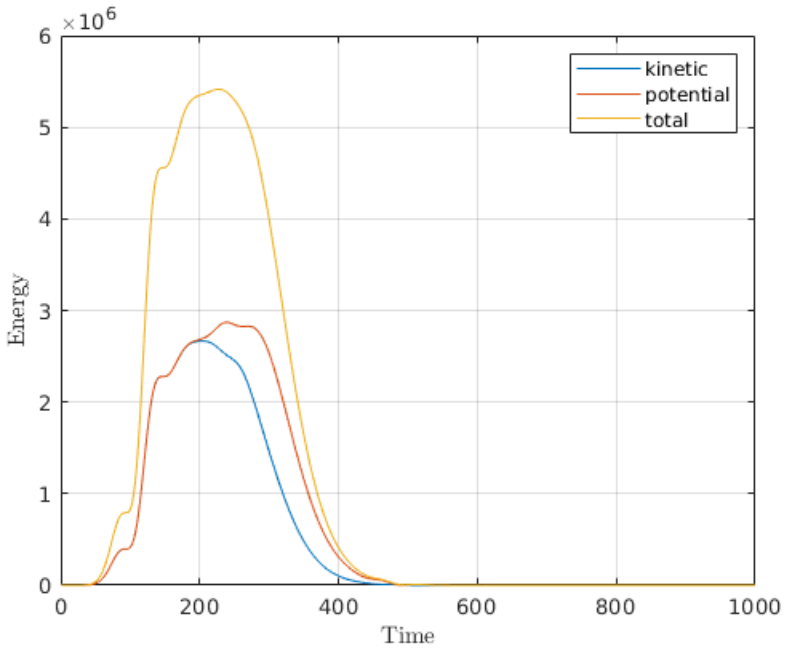

FIGURE 28 – Potential, kinetic and total energies

The energies starts growing together as the wave enters the medium. Once the wave reaches the PML, the energies start decaying rapidly and reaches a value close to 0. In fact a close analysis of the figure 28 and zooming on it, we can conclude that the energies tend to 0.

3.2 Lamb's test case

3.2.1 Description

The Lamb's test consists of an infinite half space medium and in the application of a load, given by a Ricker wave, at the surface. This context can be summarized by the figure 29. The left size disposes of symmetry conditions and the medium is surrounded on the left size and in the depth by a PML. This situation permits to simulate the propagation of seismic waves. The simulation will involves P-, S- and Rayleigh waves which are key waves in the analysis of seismic scenarios. It is known to be a good test to highlight the performance of the PML to attenuate surface waves [24].
In this test we choose the same values for the parameters of the elastic medium than in the previous test case. For the PML, we choose a value of the coefficient of reflexion $R_{pp} = 1e - 6$ to have a stronger attenuation since surface waves are more complicated to decay. The same parameters for the input Ricker wave are used. The elastic medium is a square of length 250 and the PML have a width of 200.

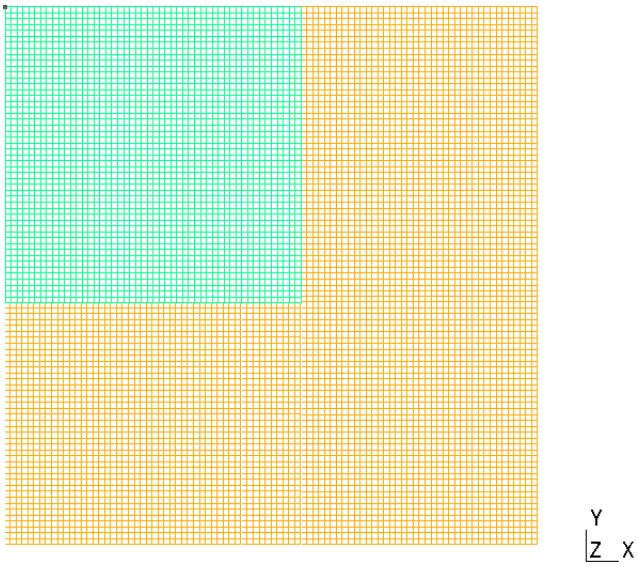

FIGURE 29 – Lamb's test

3.2.2 Analysis of the results

Using the implicit integration scheme we obtain the following results for 4 specific times. For each figure, we represented a 2D view of the medium and the PML like the one in figure 29 and the figures are colored by the magnitude of displacement. The color blue stands for a displacement equal to 0 and red for the maximum displacement.

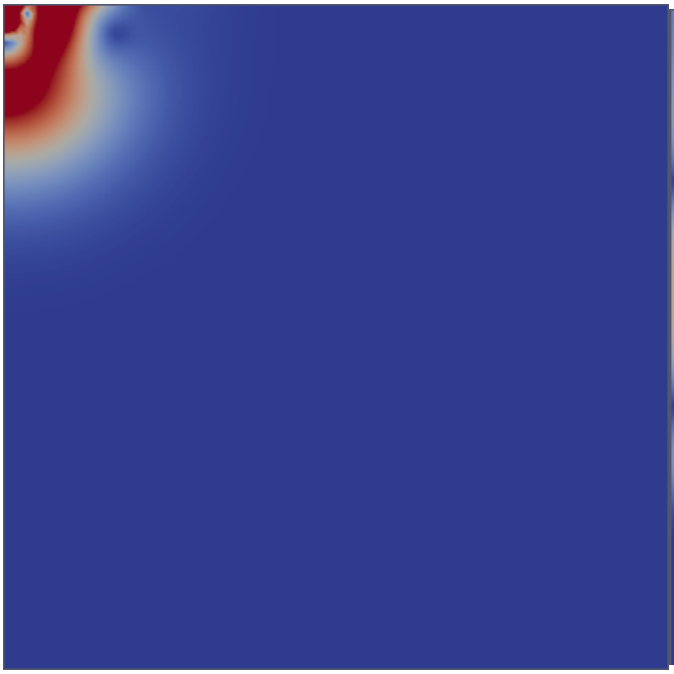

FIGURE 30 – Time 10

FIGURE 31 – Time 200

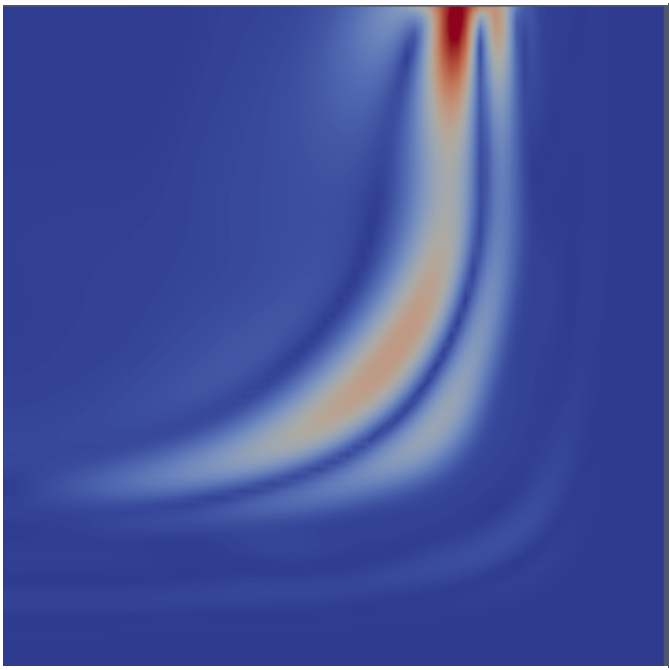

FIGURE 32 – Time 500

FIGURE 33 – Time 1000

— Figure 30 : The wave starts propagating in the elastic medium. The faster wave to propagate is the P-wave which goes into the depth of the soil.
— Figure 31 : The different waves can clearly be seen. The P-wave is near the edge of the PML located at the bottom of the medium of interest. Following the surface, the S-wave propagates toward the PML followed by the Rayleigh waves. On this figure, two of them can be seen and are represented in red because they involve the larger displacement.
— Figure 32 : The Rayleigh waves reached the PML and start to be attenuated. The S- and P-waves have already been attenuated.
— Figure 33 : All waves have been attenuated.

Let us record the displacement of a node located at the surface of the medium and at $x = 100$. The displacement are recorded along the 2 directions.

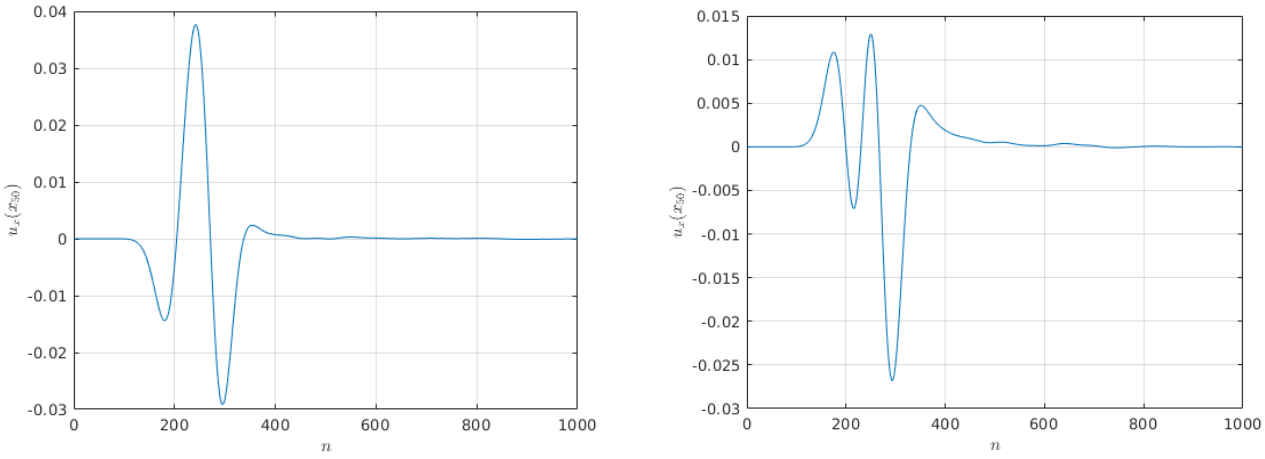

FIGURE 34 – Displacement within the x direction (left) and y direction (right)

As in the previous test case, we can observe a slight reflection corresponding to less than 1% of the initial wave. We can conclude that in term of displacement the PML is able to attenuate surface waves like Rayleigh waves. The power of attenuation of the PML can also be highlighted by the decay of the energies.

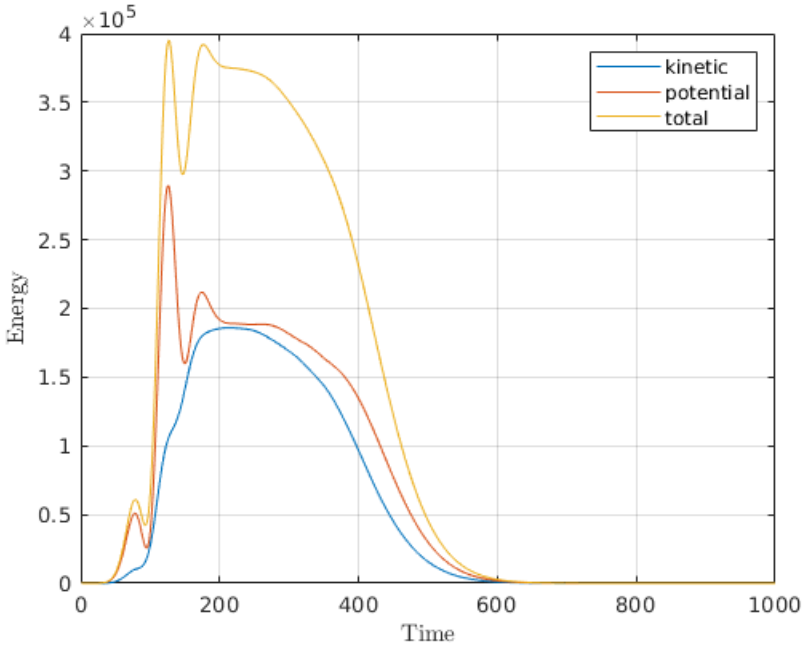

FIGURE 35 – Potential, kinetic and total energies

As we can observe on the figure 35, the energies start increasing and oscillating. Each of these oscillations is associated with the progressive arrival of the different waves. The energies seem to reach an equilibrium when all waves are propagating within the medium. Then the energies start decaying : the waves reached the PML and are attenuated. The energies tend to the value 0 when t tends to large values. In the context of seismic simulation, the analysis of the propagation of the waves can be realised considering the medium infinite since the waves are not reflected at the boundaries of the domain of interest. A careful choice of the parameters of the PML can minimize the reflexion of the wave due to the truncation interface. By its tunable ability the PML is a very good technique to simulate the propagation of waves in infinite medium.

Conclusion

The development and the analysis of the PML show two of the main aspects of the perfectly matched layers method : its power to attenuate incident waves and but also its complexity. Indeed, we have seen the full development of the equations required to construct the one dimensional PML. Starting from the simple governing equations of a linear elastodynamic problem such as the equation of motion, the constitutive equation and the strain-displacement relationship, we derived a new problem by introducing the complex coordinates and the stretching function λ. This development allowed us to obtain the strong form of the PML. Going from this formulation, we were able to construct the weak form of the PML by introducing virtual displacements in order to implement these equations using the finite element approach. Using a Newmark temporal integration method, we were capable to construct two schemes for wave propagation within the PML and therefore ensure its attenuation. A full algorithm was also presented to summarised the main steps of the scheme and the calculation of the different constitutive elements of the PML. After presenting the method that we used to prove the stability of the integration scheme associated with the PML (and therefore the scheme used to simulate the wave propagation within a PML), we have described the different elements that we can extract from the amplification matrix. From these different calculations, we also described what can be deduced about the scheme using the example of the standard element. We were able to recover well known results from the literature using this stability method. The second step was to apply this method to the PML to see if we can prove its numerical stability. The analysis of the implicit scheme associated with the PML has been proved unconditionally stable since the eigenvalues of the amplification matrix remained in the unit circle regardless of the time step considered. The explicit scheme was shown to be conditionally stable and we were able to present the critical value of the time step h for which it becomes unstable. Also, an important feature of PML was highlighted with this analysis : the attenuation introduced within the PML permits to postpone the value of the critical time step to larger values. Since the calculation and inversion of the effective stiffness matrix needed in the algorithm are expensive, one can prefer to introduce less time steps within the PML. In fact the analysis of the periodicity error showed that the increase of the time step parameter leads to a larger error but, the PML is not designed to model properly and precisely wave propagation. Its usefulness is to attenuate incoming waves. Therefore, as much as the wave does not come back in the domain of interest, the accuracy of wave propagation in the PML does not matter.

Even if this report mainly focused on the stability analysis of this particular formulation of the PML, we included a section dedicated to numerical results about two test cases. The first one, the bar test case, is a simplification of the two dimensional problem with a one dimensional view. The second test case is well known from seismologist : the Lamb's test. It represents the propagation of seismic waves within a two dimensional medium and involves 3 kinds of waves : P-, S- and Rayleigh waves. The PML has shown the ability to attenuate with efficiency the waves involved in both test cases. Also the reader and the user of the PML scheme implemented within Akantu is strongly encouraged to take advantage of the tunable ability of the PML to fit its objectives. Indeed changing the parameters of the PML such as the attenuation coefficients, the time step parameter or the lengths of the elements of the PML can impact the results and a careful choice needs to be made by the user. Of course the same dilemma between performance and accuracy has to be settle. For the PML, the accuracy has to be evaluated in term of the reflection of the wave due to the truncation interface.

In future works, a complete analysis of the computational cost of this method needs to be done : computational resources and time of execution. The explicit scheme implemented in Akantu does not support the lumping of the mass matrix reducing drastically the advantage of this latter comparing to the implicit scheme. Introducing the lumping of the mass matrix of the PML will permit the scheme to not calculate its inverse but only to make a simple matrix-vector calculation. To take advantage of the efficiency of this explicit scheme, it will be interesting to implement a coupling method within Akantu. This will permit to

choose different time steps and also different integration methods for the medium of interest and for the PML. A similar approach has been developed in [7] using Lagrange multipliers to ensure the continuity of the velocity at the interface. The implementation of such method within Akantu can be a solution to reduce the computational cost of the PML by reducing the number of time steps in the PML. This method will be able to take benefit of the ability of the PML to postpone the critical value of the time step as we have shown in the stability analysis.
Perfectly matched layers have been developed for three dimensional problems [35]. The implementation in Akantu and the stability analysis of the 3D PML can also constitute a following to this work. The field of research concerning the development and analysis of perfectly matched layer is constantly evolving and its applications can lead to the development of some fields of research in Geosciences and Civil Engineering. Since Akantu is open-source library, we strongly encourage the reader to take a look at the code and use the examples concerning the PML to reproduce the results presented in this report. They can also add their own contribution and develop the code or use the already present features in their own projects.

Références

[1] Gottlieb D. Abarbanel S. A mathematical analysis of the pml method. *Journal of Computational Physics*, 134(2) :357–363, 1997.

[2] Gottlieb D. Abarbanel S. On the construction and analysis of absorbing layers in cem. *Applied Numerical Mathematics*, 27(4) :331–340, 1998.

[3] Hesthaven J.S. Abarbanel S., Gottlieb D. Long time behavior of the perfectly matched layer equations in computational electromagnetics. *Journal of Scientific Computing*, 17(1-4) :405–422, 2002.

[4] Engquist B. and Majda A. Absorbing boundary conditions for the numerical simulation of waves. *Mathematics of computation*, 31(139) :629–651, 1977.

[5] Chopra A. K. Basu U. Perfectly matched layers for time-harmonic elastodynamics of unbounded domains : theory and finite-element implementation. *Computational methods in applied mechanics and engineering*, 192 :1337–1375, 2003.

[6] Chopra A. K. Basu U. Perfectly matched layers for transient elastodynamics of unbounded domains. *International Journal For Numerical Methods in Engineering*, 59 :1039–1074, 2004.

[7] Michael Brun, Eliass Zafati, Irini Djeran-Maigre, and Florent Prunier. Hybrid asynchronous perfectly matched layer for seismic wave propagation in unbounded domains. *Finite Elements in Analysis and Design*, 122 :1 – 15, 2016.

[8] Fauqueux S. Bécache E. and Joly .P. Stability of perfectly matched layers, group velocities and anisotropic waves. *Journal of Computational Physics*, 188(2) :399–443, 2003.

[9] Tsogka C. Bécache E., Joly P. Fictitious domains, mixed finite elements and perfectly matched layers for 2-d elastic wave propagation. *Journal of Computational Acoustics*, 9(3) :1175–1201, 2001.

[10] Liu Q.H. Chew W.C. Perfectly matched layers for elastodynamics : A new absorbing boundary condition. *Journal of Computational Acoustics*, 4(4) :341–359, 1996.

[11] Weedon W.H. Chew W.C. A 3d perfectly matched medium from modified maxwell's equations with stretched coordinates. *Microwave and Optical Technology Letters*, 7(13) :599–604, 1994.

[12] Fauqueux S. Cohen G. Mixed spectral finite elements for the linear elasticity system in unbounded domains. *SIAM Journal on Scientific Computing*, 26(3) :864–884, 2005.

[13] Tsogka C. Collino F. Application of the perfectly matched absorbing layer model to the linear elastodynamic problem in anisotropic heterogeneous media. *Geophysics*, 66(1) :294–307, 2001.

[14] Giannopoulos A. Drossaert F.H. Complex frequency shifted convolution pml for fdtd modelling of elastic waves. *Wave Motion*, 44(7–8) :593–604, 2007.

[15] Giannopoulos A. Drossaert F.H. A nonsplit complex frequency-shifted pml based on recursive integration for fdtd modeling of elastic waves. *Geophysics*, 72(2) :T9–T17, 2007.

[16] Vilotte J.-P. Festa G. The newmark scheme as velocity–stress time-staggering : an efficient pml implementation for spectral element simulations of elastodynamics. *Geophysical Journal International*, 161 :789–812, 2005.

[17] Hu F.Q. On absorbing boundary conditions for linearized euler equations by a perfectly matched layer. *Journal of Computational Physics*, 129(1) :201–219, 1996.

[18] Turkel E. Harari I., Slavutin M. Analytical and numerical studies of a finite element pml for the helmholtz equation. *Journal of Computational Acoustics*, 8(1) :121–137, 2000.

[19] Broschat S.L. Hastings F.D., Schneider J.B. Application of the perfectly matched layer (pml) absorbing boundary condition to elastic wave propagation. *Journal of the Acoustical Society of America*, 14(100) :3061–3069, 1996.

[20] Bérenger J.-P. A perfectly matched layer for the absorption of electromagnetic waves. *Journal of Computational Physics*, 114(2) :185–200, 1994.

[21] Tromp J. Komatitsch D. A perfectly matched layer absorbing boundary condition for the second-order seismic wave equation. *Geophysical Journal International*, 154 :146–153, 2003.

[22] Kallivokas L.F. Kucukcoban S. Mixed perfectly-matched-layers for direct transient analysis in 2d elastic heterogeneous media. *Computational Methods in Applied Mechanics and Engineering.*, 200 :57–76, 2011.

[23] Géradin M. and Rixen D. *Mechanical vibrations : Theory and applications to structural dynamics, second edition.* John Wiley and sons, 1997.

[24] Shuo Ma and Pengcheng Liu. Modeling of the perfectly matched layer absorbing boundaries and intrinsic attenuation in explicit finite-element methods. *Bulletin of the Seismological Society of America*, 96(5) :1779–1794, 2006.

[25] Papageorgiou A.S. Meza-Fajardo K.C. A nonconvolutional, split-field, perfectly matched layer for wave propagation in isotropic and anisotropic elastic media : stability analysis. *Bulletin of the Seismological Society of America*, 98(4) :1811–1836, 2008.

[26] Bettess P. Infinite elements. *International Journal for Numerical Methods in Engineering*, 11(1) :53–64, 1977.

[27] Liu Q.H. Perfectly matched layers for elastic waves in cylindrical coordinates. *Journal of the Acoustical Society of America*, 105(4) :2075–2084, 1999.

[28] Geers T.L. Qi Q. Evaluation of the perfectly matched layer for computational acoustics. *Journal of the Acoustical Society of America*, 100(5) :3061–3069, 1996.

[29] Ungless RL. An infinite element method, masc thesis. *University of British Columbia*, 11(1) :53–64, 1973.

[30] Gedney S.D. Roden J.A. An efficient fdtd implementation of the pml with cfs in general media. *IEEE Antennas Propagat. Soc. Int. Symp.*, 3(2000) :1265–1362, 2000.

[31] Lenti L. Semblat JF and Gandomzadeh A. A simple multi-directional absorbing layer method to simulate elastic wave propagation in unbounded domains. *International journal for numerical methods in engineering*, 2010.

[32] Belytschko T. *Nonlinear finite elements for continua and structures.* Chichester : Wiley, 2013.

[33] Chew W.C. Teixeira F.L. On causality and dynamic stability of perfectly matched layers for fdtd simulations. *IEEE Trans. Microwave Theory Tech.*, 47(6) :775–785, 1999.

[34] Yefet A. Turkel E. Absorbing pml boundary layers for wave-like equations. *Applied Numerical Mathematics*, 27(4) :533–557, 1998.

[35] Basu U. Explicit finite element perfectly matched layer for transient three-dimensional elastic waves. *International Journal For Numerical Methods in Engineering*, 44 :151–176, 2008.

[36] Tang X. Wang T. Finite-difference modeling of elastic wave propagation : a nonsplitting perfectly matched layer approach. *Geophysics*, 68(5) :1749–1755, 2003.

[37] H. P. Cherukuri X. Ling. Stability analysis of an explicit finite element scheme for plane wave motions in elastic solids. *Computational Mechanics*, 29 :430–440, 2002.

[38] Liu Q.H. Zeng Y.Q., He J.Q. The application of the perfectly matched layer in numerical modeling of wave propagation in poroelastic media. *Geophysics*, 66(4) :1258–1266, 2001.

[39] Ballmann J. Zhang Y.-G. Two techniques for the absorption of elastic waves using an artificial transition layer. *Wave Motion*, 25(1) :15–33, 1997.